Direct Measurement of Patellofemoral Contact Force

by
Cheri Geldenhuys

Thesis presented in partial fulfilment of the requirements for the degree of Master of Engineering (Mechanical) in the Faculty of Engineering at Stellenbosch University

Supervisor: Dr. Jacobus Hendrik Müller
Co-supervisor: Prof. David Jacobus van den Heever

March 2020

Declaration

By submitting this thesis electronically, I declare that the entirety of the work contained therein is my own, original work, that I am the sole author thereof (save to the extent explicitly otherwise stated), that reproduction and publication thereof by Stellenbosch University will not infringe any third party rights, and that I have not previously, in its entirety or in part, submitted it for obtaining any qualification.

Date: ..... Signature: .....

Abstract

Osteoarthritis is a prevalent disease that affects millions of people around the world. The most effective treatment is a total knee arthroplasty. However, post-operative patellofemoral problems do arise, such as anterior knee pain, which affects up to 23% of patients. The cause of post-operative anterior knee pain remains unknown. It has been noted that patients with patellar buttons that were overstuffed during surgery are more likely to suffer anterior knee pain. This has led to the theory that overstuffing might be a cause of post-operative patellofemoral pain. It is believed that the thickness of the patellar implant may have an effect on the contact force experienced by the patellofemoral joint. The present study aimed to directly measure the contact force experienced by the patellar button prosthesis used in total knee arthroplasty, in a simulated environment, using a force sensor. The results of the contact force experienced by patellar buttons of different thicknesses used in total knee arthroplasty were then compared. The difference in the thickness of the patellar buttons proved to have a significant effect on the simulated patellofemoral contact force. This may be proof that overstuffing the patellofemoral joint could significantly increase the patellofemoral contact force, leading to further problems.

Uittreksel

Osteoartritis is 'n algemene siekte wat miljoene mense regoor die wêreld affekteer, en die mees effektiewe behandeling is totale knie-artroplastiek. Hoewel totale knie-artroplastiek een van die suksesvolste operasies is, ontstaan post-operatiewe patellofemorale probleme, soos anterieure kniepyn, wat tot 23% van pasiënte raak. Die oorsaak van anterieure kniepyn ná totale knie-artroplastiek is onbekend. Pasiënte met patellêre inplantate wat tydens die operasie oormatig oorvul is, is meer geneig om patellofemorale kniepyn ná die operasie te hê. Dit het gelei tot die teorie dat oormatige vulling van die patellêre inplantaat 'n oorsaak van patellofemorale pyn kan wees. Daar word geglo dat die dikte van die patellêre inplantaat 'n invloed kan hê op die kontakkrag wat die patellofemorale gewrig ervaar. Die huidige studie was daarop gemik om die kontakkrag wat deur die patellêre inplantaat in 'n totale knie-artroplastie ondervind word in 'n gesimuleerde omgewing met behulp van 'n kragsensor te meet. Die kontakkrag wat deur patellêre inplantate van verskillende diktes wat in totale knie-artroplastiek gebruik word, is vergelyk. Die verskil in die dikte van die patellêre inplantate het 'n beduidende uitwerking op die gesimuleerde patellofemorale kontakkrag gehad, wat daarop dui dat oorvulling van die patellofemoral gewrig die patellofemorale kontakkrag aansienlik verhoog, wat tot verdere probleme kan lei.

Acknowledgements

First, I want to thank my supervisor Dr Müller for granting me this project and for all his patience, guidance, help, and the privileges he afforded me along the way. I have enjoyed this project so much and could not have done any of it without him.

I also want to thank my co-supervisor, Prof van den Heever, for his insights and suggestions.

I thank Dr Eric Ledet for the opportunity to work with the sensor design and to spend time at RPI. I would also like to thank Dustin Schroeder for all his help with the sensor design.

I thank Mr Ferdi Zietsman and Mr Graham Hamerse for the manufacturing of the test rig.

I thank Prof Kidd for his advice and support in analysing the data.

I thank Stephen Klue for his help with the vapour deposition process in coating the force sensors.

I thank Anneke Bester for the help with the antenna and network analyser.

I thank all my friends, family, and BERG for their support throughout this project, with special thanks to Jan Vorster, Joka Plotz, Peter Kageler, and Andreas Werle van der Merwe for all their help with my experiments and writing.

I thank my parents and my brother for giving me the chance to further my studies and for always supporting and helping me throughout this project.

I thank my heavenly Father for blessing me with this journey.

Dedicated to my mother, father and brother.

Table of contents

List of figures

Page

List of tables

1 Introduction

1.1 Background and motivation

Osteoarthritis is a prevalent disease that affects millions of people around the world (Vos *et al.*, 2012). Currently, the most effective treatment is a total knee arthroplasty (Becker *et al.*, 2011). While this is one of the most successful surgeries, post-operative patellofemoral problems such as anterior knee pain do arise, affecting up to 23% of patients (Matz *et al.*, 2019). The cause of anterior knee pain remains unknown, but current research suggests the cause is multifactorial (Matz *et al.*, 2019). Patients with patellar buttons that were overstuffed during surgery, meaning the femoral or patellar component is larger than the amount of bone removed during surgery, are more likely to suffer anterior knee pain (Matz *et al.*, 2019). Current research supports the theory that overstuffing is the cause of post-operative patellofemoral pain, and that the thickness of the patellar implant may have an effect on the contact force experienced by the patellofemoral joint as demonstrated in Figure 1.

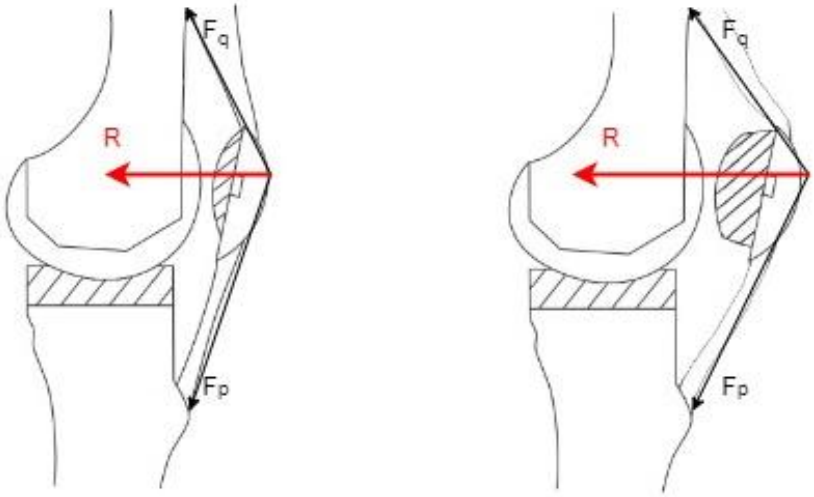

Figure 1: Forces created by thinner and thicker patellar buttons. The image on the left shows a thinner patellar button and the resulting reaction force (R) created by the quadriceps muscle force (F_q) and the patellar ligament force (F_p). The image on the right shows an exaggerated, thicker patellar button, which results in a larger reaction force.

This is possibly due to pain receptor activation as a consequence of the increased forces experienced by the patellar button due to overloading. It is not yet known how different patellar button thicknesses influence the contact forces experienced by the patellofemoral joint. While a variety of force estimation methods exist, patellofemoral forces are yet to be measured *in vivo*. Therefore, this study aimed

to develop a suitable method to measure the patellofemoral contact forces *in vivo* in future projects.

1.2 Aims and objectives

The study aim was to directly measure the contact forces experienced by the patellar button prosthesis used in total knee arthroplasty in a simulated environment. The results were then be used to compare the contact force experienced by the patellar buttons of varying thicknesses used in total knee arthroplasty.

The study objectives were as follows:

Research Objective 1: Design different configurations of an existing force sensor design that can directly measure the patellofemoral contact force experienced by the patellar button prosthesis.

Research Objective 2: Design an experiment set-up to calibrate and characterise the force sensor for use in further testing.

Research Objective 3: Design a test rig to measure the contact forces experienced by patellar buttons of different thicknesses.

Research Objective 4: Determine the effect of the different thicknesses of patellar buttons on patellofemoral contact force in a simulated environment.

2 Literature review

This chapter reviews the anatomy of the knee (Section 2.1), osteoarthritis and end-stage osteoarthritis treatment (Section 2.1), total knee arthroplasty (Section 2.2), patella button designs (Section 2.3), post-operative anterior knee pain (Section 2.4), and relevant prior research (Section 2.5).

2.1 Anatomy of the knee

The knee joint is the largest joint in the human body and permits extension and flexion. Extension refers to the movement of the joint using extensor muscles (in this case, the quadriceps muscles) toward a more obtuse angle. Flexion refers to the movement of the joint using flexor muscles (in this case, the hamstring muscles) toward a more acute angle. As the junction between the femur and tibia, the knee involves the tibia, femur, fibula, and patella, as shown in Figure 2. Also known as the kneecap, the patella is found at the anterior knee, where it protects and supports the interior knee joint. The patella articulates with the trochlea of the femur; together, they form the patellofemoral joint. The trochlea is the pulley-like groove at the end of the femur. The trochlea guides the way the patella rolls over the femur under flexion or extension (Moses, 2013).

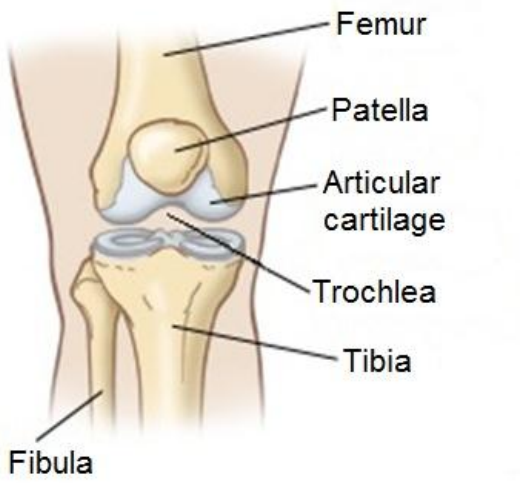

Figure 2: Bones of the knee joint (Fairview, 2019).

The motions of the knee joint are driven by its attendant tendons, ligaments, and muscles. With muscles driving movement, tendons connect the muscles to bones, while ligaments join the bones together to form a joint and create stability. As shown in Figure 3, the quadriceps muscle is responsible for knee extension. The quadriceps muscle is attached to the quadriceps tendon, which, in turn, is attached to the patella. The patella is attached to the patellar ligament, which is attached to the tibia.

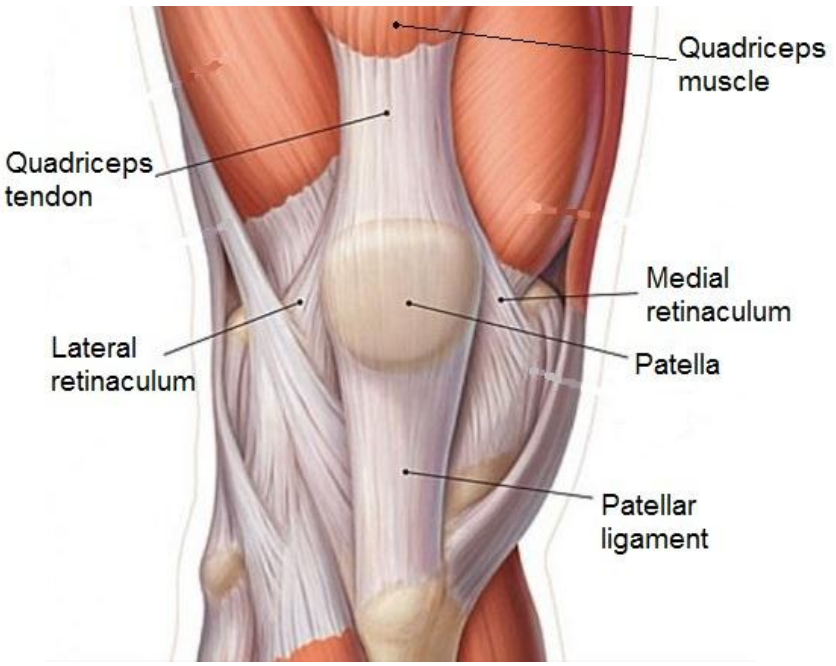

Figure 3: Muscles and ligaments surrounding the patella (Digikalla, 2017).

The patella is the largest sesamoid bone in the human body (Scott *et al*., 2012), with an approximate length of 40 mm to 45 mm and an approximate width of 50 mm to 55 mm. Across its length, the thickness of the patella varies significantly, with a maximum at the highest point being between 20 mm and 25 mm *(Reider et al.*, 2019). The patella's function is to act as a spacer to increase the extensor moment arm of the quadriceps muscle, as well as to act as a lever for extension and flexion (Browne *et al.*, 2005). Other primary functions of the patella include assisting the quadriceps muscle group to extend the lower leg and to keep the knee stable while flexion takes place (Hungerford *et al*., 2019). The patella has both active and passive stabilisers to ensure its stability (Navarro *et al*., 2010). The patellar tendon acts as a passive stabiliser, while the quadriceps muscles are an active stabiliser, also responsible for the movement of the patella.

During knee flexion, the patella shifts laterally (Horng-Haung *et al.*, 1996). The contact area of the patella moves from distal to proximal as the flexion angle increases (Horng-Haung *et al.*, 1996). The force the patella experiences increases as flexion increases, spreading larger forces over a larger area. This is true only if the extension is free and does not meet resistance (Scott *et al*., 2012).

Studies have shown that the patella increases the extension force by up to 50%. This results in very large forces present in the patellofemoral joint. Studies have also indicated that the forces present at the patella can be up to 7.6 times the force of the body mass; however, this has not yet been proven (Matz *et al.*, 2019). The patella also increases the surface area that distributes the force, and assists in centralising the forces of the extensor mechanism (Matz *et al.*, 2019).

As mentioned previously, the medial and lateral retinacula primarily stabilise the patella, but another important function of the retinaculum is that it resists the stresses the knee experiences whilst flexing, and thus shares in the load that is exerted on the patella ligament (Powers *et al*., 2006). The only muscle to which the patella is connected is the quadriceps muscle, and, thus, the only forces exerted on the patella are those of the quadriceps muscle and the patellofemoral ligament. The patella acts as a lever for the knee while flexion and extension takes place; thus, reaction forces are formed due to the forces and moments of the quadriceps muscle and the patella ligament (Powers *et al*., 2016). These forces are illustrated in Figure 3.

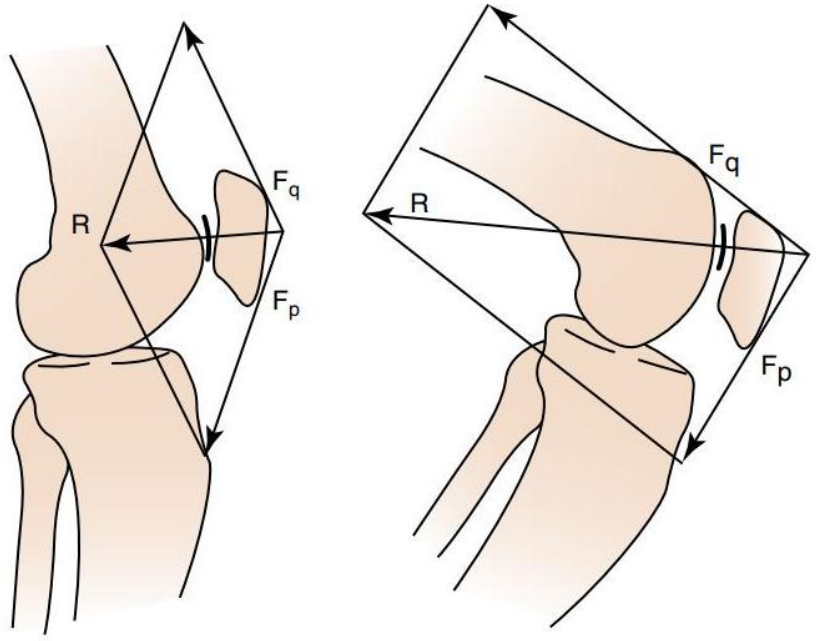

Figure 4: Reaction forces in the patellofemoral joint (Powers *et al.*, 2016)*. The left image is that of an extended knee, and the right image is that of a flexed knee, showing the difference in the magnitude of the reaction force.* F_q *represents the force created by the quadriceps muscle,* F_p *represents the force created by the patellar ligament, and R represents the reaction force.*

The reaction force that is formed can be seen as the amount of force that pushes the patella onto the trochlea. Thus, the articular cartilage between the patella and femur is placed under pressure (Powers *et al.*, 2016). The reaction force is dependent on the amount the knee is flexed or extended, and also on how much force the quadriceps muscle exerts on the patella.

Osteoarthritis is a very common disease, resulting the destruction of cartilage in a joint over time (Arden *et al*., 2006; Vos *et al.*, 2012). Risk factors include age, gender, bone density, genetics, and nutrition (Arden *et al*, 2006), with women over the age of 60 years being the most commonly affected (Glyn-Jones *et al*., 2015).

Osteoarthritis manifests in joint symptoms, structural pathology, or a combination of the two. The main symptoms of the disorder are pain and stiffness in joints. The condition is most prevalent in the knee joint, and causes pain, swelling, and stiffness, while limiting the motion of the joint (Becker *et al.*, 2011). In severe cases, joint functionality can be lost altogether (Glyn-Jones *et al.*, 2015). The diverse joint pathology can include loss of articular cartilage, focal damage osteophytes, and inflammation. Osteoarthritis is widely seen as an age-related disorder due to injury in the joint. Its main features are the loss of articular cartilage and changes in the bone of the joint.

Evidence suggests that limb alignment such as varus and valgus knees, depicted in Figure 5, can increase the risk of osteoarthritis development and progression, due to the vulnerable regions being overloaded (Glyn-Jones *et al.*, 2015). However, most individuals with abnormal joint biomechanics do not develop the disease (Glyn-Jones *et al.*, 2015). Injury of the knee can increase the risk of knee arthritis by more than four times by causing cartilage- or bone damage. Obesity can increase the risk of knee arthritis by a factor of three, due to overloading of these weight-bearing joints (Glyn-Jones *et al.*, 2015).

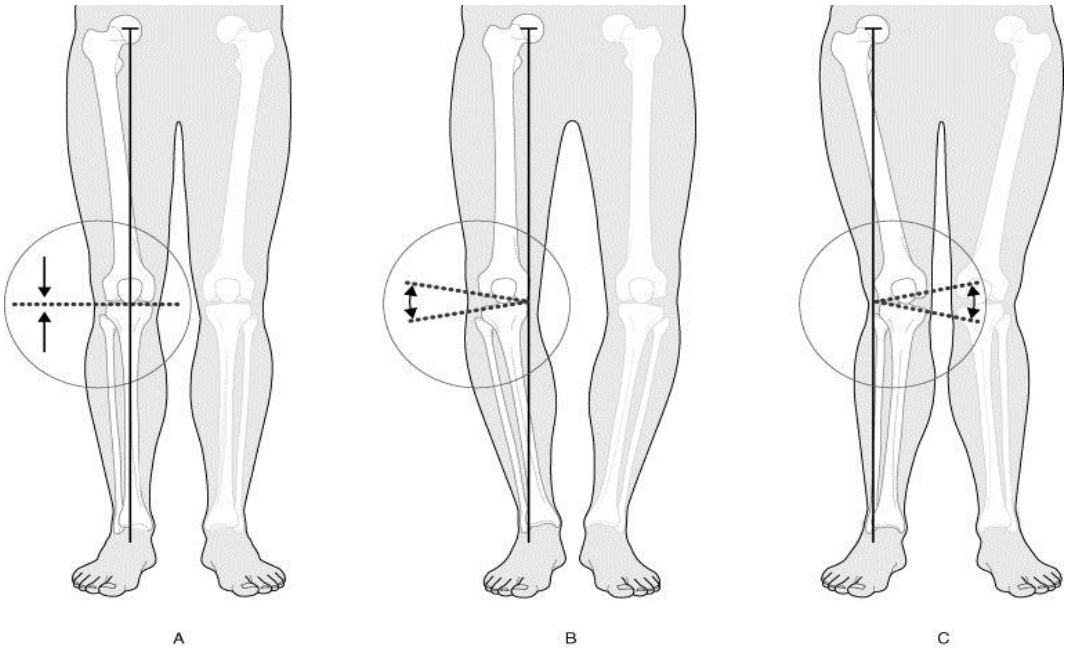

Figure 5: Schematic of the difference between a normal knee alignment (A), varus knees (B), and valgus knees (C) (Carreiro, 2009).

Treatment of the disease involves pain management or, for end-stage osteoarthritis, joint replacement. Total knee arthroplasty is the most effective solution for osteoarthritis in the knee (Becker *et al.*, 2011). Although a multitude of other knee conditions can lead to total knee arthroplasty, the most common reason for total knee arthroplasty is osteoarthritis (Becker *et al.*, 2011).

2.2 Total knee arthroplasty

For patients suffering from end-stage knee osteoarthritis, total knee arthroplasty is the most successful and cost-effective option (Roussot *et al*., 2019; Tanikawa *et al*., 2017). Total knee arthroplasty refers to the reconstruction or replacement of the knee components with metal or plastic prostheses. The surgery replaces the surfaces of the knee components, as shown in Figure 6, to reduce pain and increase the stability of the joint (Putman *et al*., 2019).

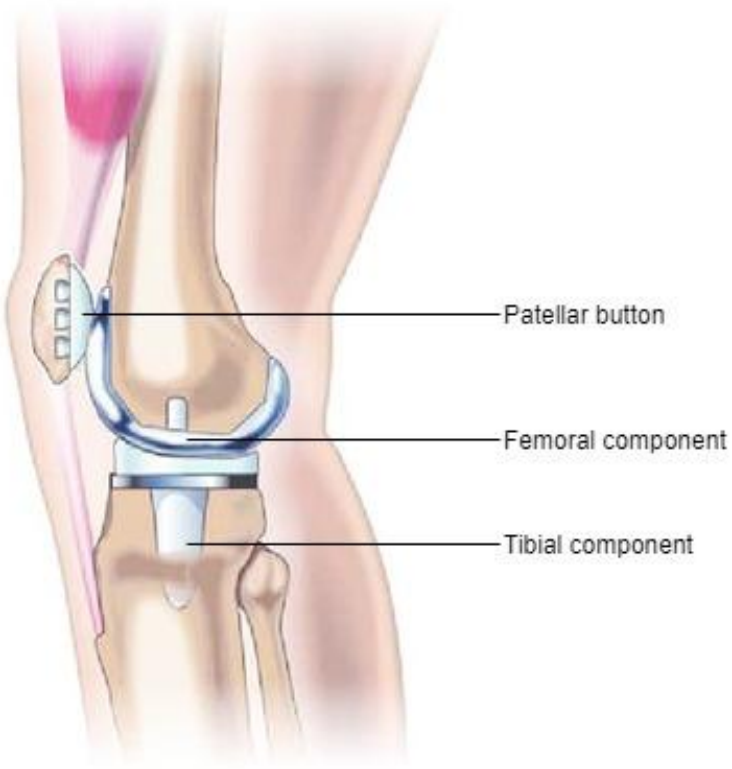

Figure 6: The knee after total knee arthroplasty, showing the three components of the knee that were replaced (Schindler, 2012).

While total knee arthroplasty has improved in terms of prosthetic design, surgical procedures, and the use of robot-assisted surgery, patellofemoral components have thus far been neglected (Roussot *et al*., 2019). Although the prostheses for total knee arthroplasty are well developed, patellofemoral joint problems still arise postoperatively (Matz *et al.*, 2019). The patellofemoral articulation is a very important part of total knee arthroplasty, and is indicative of whether the surgery was successful (Roussot *et al.*, 2019).

Post-operative complications arise regardless of whether or not the patella was resurfaced. Such complications include anterior knee pain, maltracking, and fracturing of the patella (Matz *et al.*, 2019). In the past, patellofemoral complications

were the cause of about half of revision surgeries, and the problem remains challenging (Matz *et al.*, 2019). Pain after total knee replacement is one of the most difficult post-operative issues (Becker *et al.*, 2011). The number of patients receiving total knee replacements keeps increasing, with a concomitant increase in the number of patients experiencing post-operative pain. Patients have high expectations of the surgery with regard to post-operative daily activities, with up to 85% of patients expecting to be pain free afterwards. Unfortunately, only about 43% of patients are fully pain free postoperatively (Becker *et al.*, 2011).

Total knee replacements initially did not include patellar resurfacing, but it became apparent that anterior knee pain was present following the majority of these procedures (Putman *et al*., 2019). However, after patella resurfacing was introduced, several other complications arose that are difficult to treat (Putman *et al.*, 2019). Resurfacing the patella reduces the contact area between the patellar button and femoral component to only 40% of the native contact area (Putman *et al.*, 2019). This, in turn, results in an increase in contact stress, which may result in problems such as component loosening (Putman *et al.*, 2019). When a surgeon does decide to resurface the patella, the surgeon will try to keep the resurfaced patellar thickness as close as possible to that of the native patella. Proponents of the resurfacing technique maintain that resurfacing the patellar button reduces the chance that the patient will need to undergo a second operation, and that it prevents post-operative complications such as pain and maltracking (Pierce *et al.*, 2019). They also hold that patients are less likely to experience anterior knee pain (Alcerro *et al*., 2017). Surgeons debate whether resurfacing the patella during total knee arthroplasty surgery should be compulsory.

Very little data exist on the effect the thickness of the patellar button has on the knee's range of motion following total knee arthroplasty. Surgeons tend to give more attention to the preparation of the tibial or femoral components than the patellar component when preparing for a total knee replacement surgery. It has been proven that patients experience less anterior knee pain if the patella was resurfaced during the surgery (Hamilton *et al.*, 2017). Surgeons generally try to use a patellar button whose thickness will protect the extensor mechanism as much as possible. If the patellar button is too thin, it can disrupt the extensor mechanism, whereas a thicker patella or overstuffing the patella will result in the knee joint being too stiff, and anterior knee pain is more likely to result (Hamilton *et al.*, 2017).

It was found that a thinner patella (< 12 mm) will not necessarily result in the fracturing of the patella or other complications; therefore, the surgeon can make the resurfaced patella thinner than the native patella, although this is still not desirable (Hamilton *et al.*, 2017). When the native patella is very thin, it is not always possible to keep the thickness the same when resurfacing the patella. The knee has a better range of motion when the thickness of the patellar button is kept as close as possible to that of the native patella, or thinner (Hamilton *et al.*, 2017). Although multiple studies have been done on patellar button thickness, it remains

undetermined whether it is related to post-operative complications (Pierce *et al.*, 2019).

2.3 Patellar buttons

When resurfacing the patella, a patellar button is used as the prosthesis, as shown in Figure 6. Several patellar button designs exist, as shown in Figure 7, with the basic designs being dome-shaped, anatomical, and cylindrical, each with variations (Roussot *et al*., 2019).

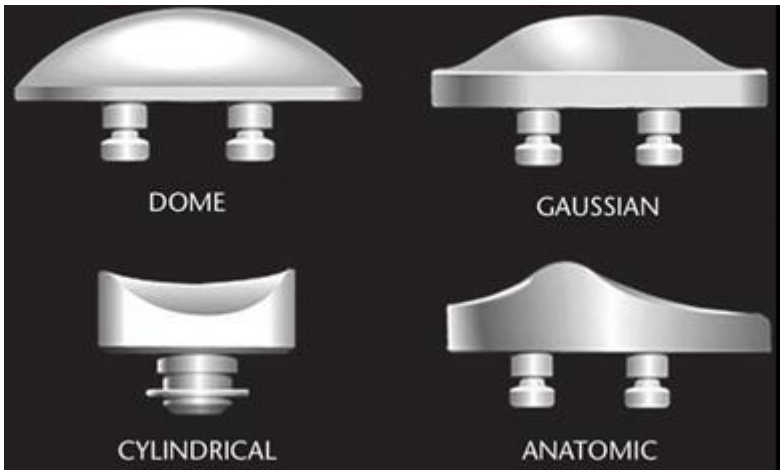

Figure 7: The different shapes of patellar buttons that have been researched and used (Roussot *et al*., 2019).

The anatomical prosthetic option has shown the best results *in vitro* with regard to contact stress, but the design may cause instability, as well as wear and shear stress between bone and the implants, causing anterior knee pain (Roussot *et al*., 2019). The dome-shaped design is ideal for the shape of the femoral component, but problems may arise, as the design may cause higher contact stress, resulting in increased wear. The Gaussian shape or modified dome typically experiences the least contact force. The dome shape and its variations remain the best and most commonly used patellar button design.

In total knee arthroplasty, the patellar component is usually made of Polyethylene (Roussot *et al*., 2019). While the material does not obviate complications such as wear due to large forces, chances of catastrophic wear are very slim (Matz *et al.*, 2019). Other factors adding to the popularity of the dome design are the ease of application of the patellar button, its high success rate, and the reduced risk of malalignment (Matz *et al.*, 2019).

2.4 Anterior knee pain

One of the biggest problems after total knee arthroplasty is patellofemoral complications, which include anterior knee pain. Evidence suggesting that resurfacing the patella reduces anterior knee pain has emerged (Putman *et al.*, 2019).

Unfortunately, not all patients are satisfied with the results of a total knee arthroplasty, as they suffer anterior knee pain post-operatively (Alcerro *et al.*, 2017). Up to 23% of patients have anterior knee pain after total knee arthroplasty surgery (Kaneko *et al*., 2018; Matz *et al.*, 2019). Research suggests that the cause for anterior knee pain is multifactorial (Matz *et al.*, 2019).

Anterior knee pain can possibly be due to factors such as the kinematics of the patella changing after total knee arthroplasty, which could be due to the varying thickness of the cartilage of the patella of different patients, as well as the design of the new patellar implant, which can change the tilt of the original patella (Tanikawa *et al.*, 2017). Although a few possible factors causing anterior knee pain are suspected, the cause of this phenomenon is not yet proven. It is, however, considered likely that the higher pressure experienced by the patella due to the change in kinematics of the patellar button is a possible cause of the condition (Tanikawa *et al.*, 2017).

Multiple studies have been conducted on the outcome of increased pressure on the patella after total knee arthroplasty, as well as how the kinematics of the patella are changed during the surgery, but very few studies compared the changes to clearly show the difference after patellar protheses were implanted (Tanikawa *et al.*, 2017).

Overstuffing is theorised to be one of the factors contributing to anterior knee pain (Matz *et al.*, 2019). The term refers to the femoral or patellar component being larger than the amount of bone removed. In theory, an overstuffed patellar may lead to larger patellofemoral forces, as depicted in Figure 1, and anterior knee pain (Matz *et al.*, 2019).

Postoperative anterior knee pain ranges from mild to acute and can greatly influence the quality of life of those living with the condition, affecting their performance of everyday tasks such as walking and climbing stairs. The cause of anterior knee pain is multifactorial but can be divided into mechanical and functional problems. It is very likely that problems in the patellofemoral mechanics, such as increased pressure at the extensor mechanism, will lead to the patella being overloaded with forces (Petersen *et al*., 2014).

It is widely speculated that the forces and loads exerted on the patella are the biggest cause of patellofemoral pain (Brechter *et al*., 2002; Powers *et al.*, 2016). The patellofemoral joint is exposed to the largest forces and loads in the entire

body. Studies have shown that the reaction forces through the patellofemoral joint for level walking are roughly equal to the person's body weight. These reaction forces increase to about 3.8 times the person's body weight while ascending or descending stairs, and reaches about seven times the person's body weight while running (Brechter *et al*., 2002; Powers *et al.*, 2016).

2.5 Previous studies

Previous studies have focused on the influence of patellar button thickness on the knee's range of motion after total knee arthroplasty, as well as the effects on the different ligament attachments to the patella (Alcerro *et al.*, 2017). However, few studies have been done on how patellar button thickness affects patellofemoral contact forces. Studies have found that an increase in patellar thickness does indeed affect the range of motion of the knee (Alcerro *et al.*, 2017). The femoral and tibial components of total knee arthroplasty rarely cause problems, but the patellofemoral component does cause some problems. It was found that these problems are largely the cause of the patellofemoral stress; therefore, it is important to directly measure the patellofemoral direct contact force (Kovacevic *et al*., 1995). Many methods exist to estimate these forces, but the forces have yet to be measured *in vivo*. Estimates have been made with mathematical models and *in vitro* testing, but the results have not yet been validated (Dion *et al*., 2015).

Oishi *et al*. (1996) conducted a study on the effects of patellar implant thickness on the compressive force. The experiments involved dissecting the joint capsules of cadaver knees of similar health, preserving only the relevant ligaments. The cadaver knees underwent standard total knee arthroplasty, with special care taken to measure the native patella thickness. Patella resurfacing was done using modular polyethylene domes mounted to metal plates with customized sections to insert the force transducer, screwed into a transducer, as shown in Figure 8.

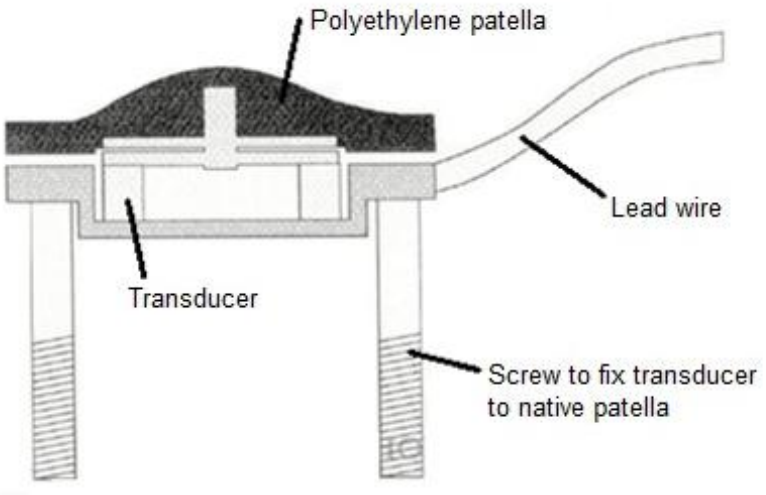

Figure 8: Schematic of the force transducer used by Oishi et al. (1996).

The patellar buttons were chosen to recreate the native patella thickness, with variations that add 2 mm and 4 mm. The knees were mounted onto an Oxford Knee Testing Rig, shown in Figure 9, that exerted a hip load of 44 N, where the patellar forces were measured from 0^0 to 95^0.

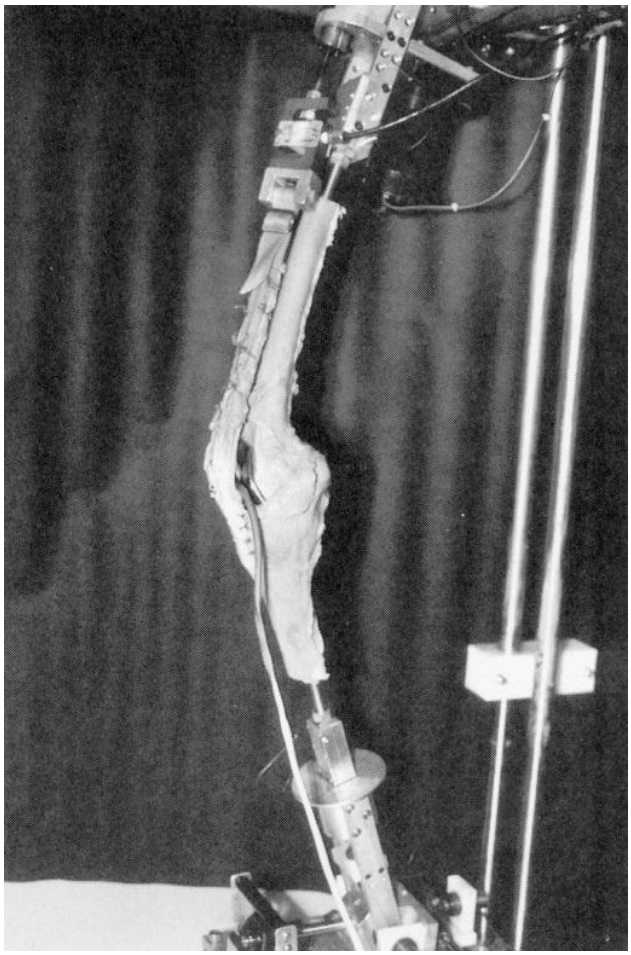

Figure 9: A cadaveric knee being tested in an Oxford knee rig, as described in the study of Oishi et al. (1996).

The results showed no significant differences in patellofemoral compressive forces between the different thicknesses. Since the external load was kept constant, the results were considered a consequence of the lever arm being longer when increasing the thickness of the patellar button, which resulted in less quadriceps force needed to extend the knee. During these experiments, the fact that the medial retinaculum was only partially closed (since the transducer cable had to exit the knee) caused some inconsistency in the results (Oishi *et al.*, 1996). Oishi *et al*. (1996) found no significant differences between the standard patellar button, the 2 mm thicker patellar button, and the 4 mm thicker patellar button.

In a study done by Hsu *et al*. (Horng-Haung *et al.*, 1996), the influence of patellar thickness on patellofemoral contact characteristics after total knee arthroplasty

was determined using cadaver specimens. A force transducer embedded between the patellar component and a metal-backed plate were used in the experiments.

As shown in Figure 10, the study found that the patellofemoral contact force was higher with an increase in knee flexion, and more force was present when using thicker patellar buttons (Horng-Haung *et al.*, 1996).

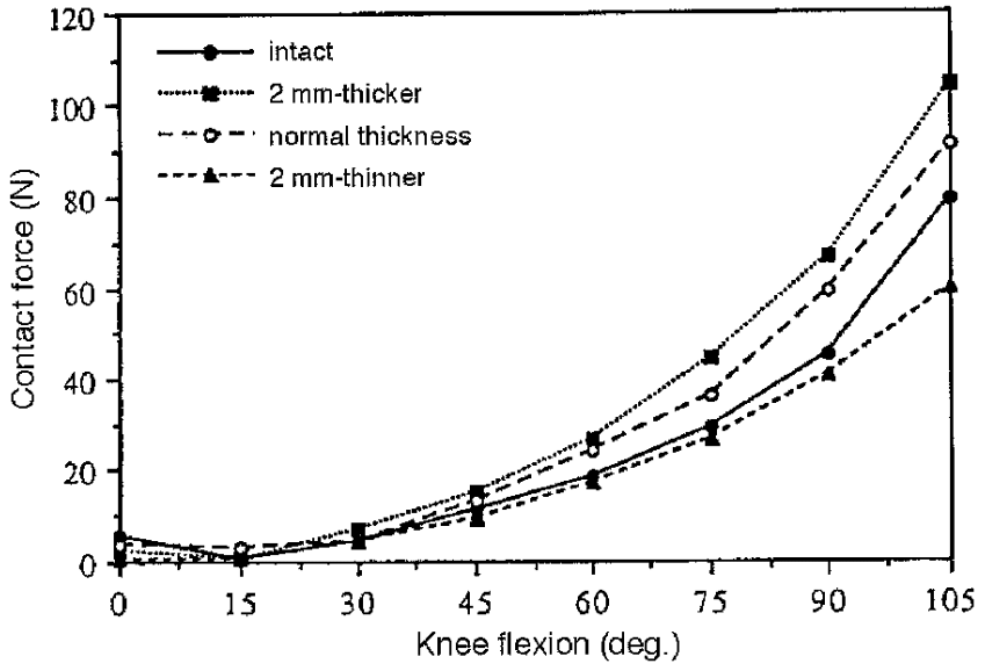

Figure 10: Patellofemoral contact force at different degrees of knee flexion obtained by Hsu et al. (Horng-Haung *et al.*, 1996).

Similar studies have been done using the same force transducer. A study by Browne *et al*. (2005) to measure patella contact force directly also used a force transducer, incorporated into the patella in the same way.

A study by Reuben *et al*. (1991) compared the effect of different thickness patellae of cadavers on patellar strain using a uniaxial strain gauge, as described in Figure 11. The results showed a significant increase in patellar strain when the bony patellar was less than 15 mm, as shown in Figure 12.

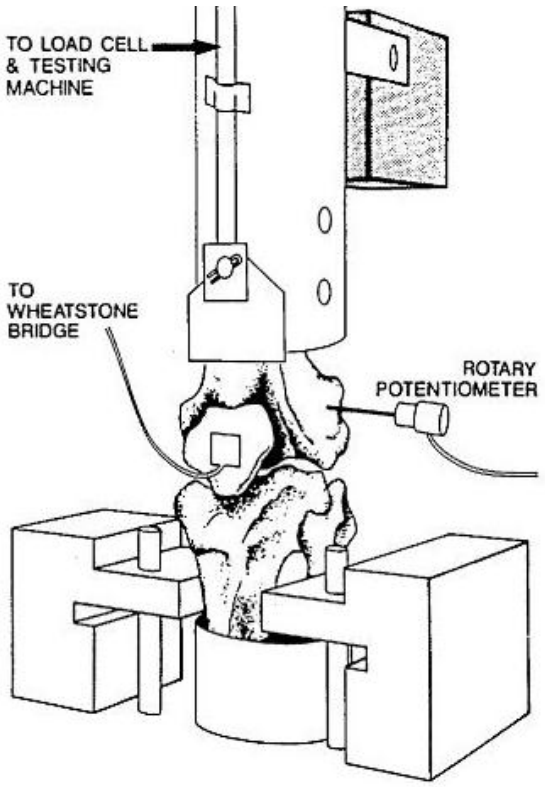

Figure 11: Experiment set-up of Reuben et al. (1991) to measure patellar strain.

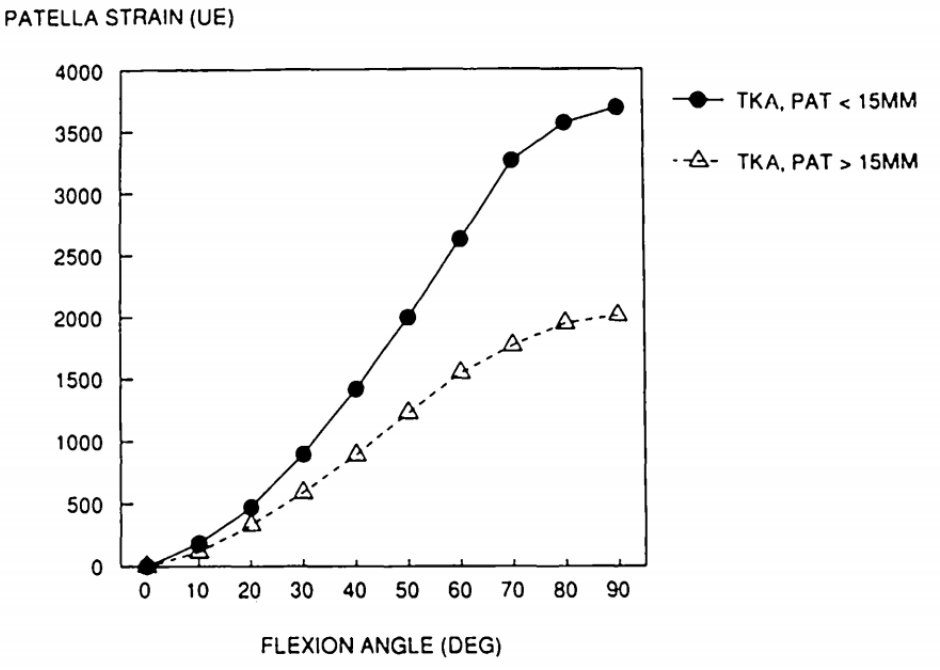

Figure 12: The effect patellae of different thicknesses on patellar strain, as documented by Reuben et al. (1991).

Previous studies attempting to measure the direct contact force included the use of strain gauges and pressure-sensitive film. Xu *et al*. (2007) tested the effects of patellar resurfacing on contact area and stress using pressure-sensitive films called 'Fuji film', shown in Figure 14. These tests were also conducted using a rig based on an Oxford Knee Rig design, shown in Figure 13, and the specimen was loaded with 30 kg (Xu *et al.*, 2007).

Figure 13: The specimen being tested on a rig exerting 30 kg to the quadriceps muscle (Xu *et al.,* 2007).

In using pressure-sensitive films like Fuji films, two films (a donor and a receiver) are placed on top of one another in the pressure measurement area. The ink from the donor film is deposited onto the receiver film where pressure is present. The darkness of the ink indicates the amount of pressure. However, pressure-sensitive films are sensitive to humidity and fluids, and can only be used once, making them unsuitable for *in vivo* testing. The results of the study of Xu *et al*. (2007) showed that resurfacing of the patella during total knee arthroplasty alters the pressure the patellofemoral joint experiences, as well as the contact area.

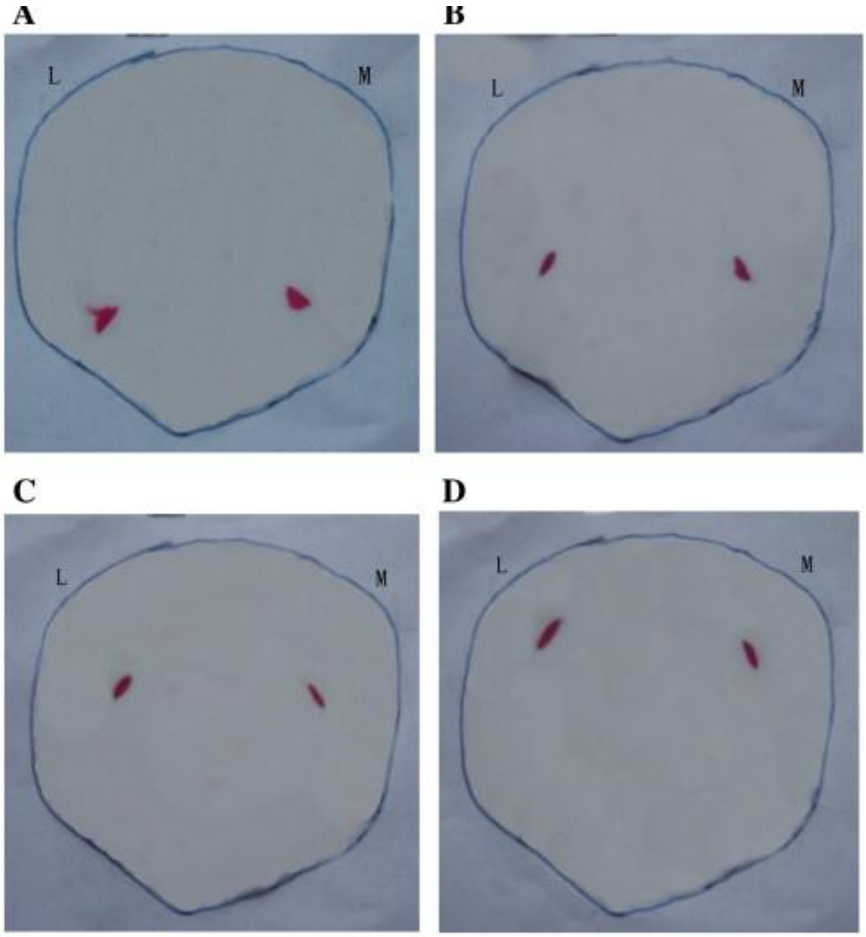

Figure 14: Fuji films showing the contact pressure of a resurfaced patella. The medial (M) and lateral (L) sides are indicated. The tests were repeated at a knee flexion of 30 ^{0}(A), 60 ^{0}(B), 90 ^{0}(C), and 120 ^{0}(D).

Other studies (Konno *et al*., 2014; Sawaguchi *et al*., 2010; Terashima *et al.*, 2015) used ultrathin force transducers, embedded between the patellar button and a metal plate, which were placed against the bone surface, similar to what is shown in Figure 8. This method only measures patellofemoral stress intraoperatively, with no external force from the quadriceps muscle present. Load cells of the same shape as the patellar button have also been used to measure patellofemoral forces intraoperatively (Kaneko *et al.*, 2018). These measurements can be done through the full range of movement.

A study by Miller *et al*. (1998) compared patellofemoral force of the native knee to patellofemoral force after total knee arthroplasty. The patellofemoral force was measured by replacing it with a measured tensile force. A cable was attached to the anterior of the patella at point P, as shown in Figure 15. The tension in the cable was increased until the patella was lifted slightly, which meant the tensile force in the cable was equal to the patellofemoral force. A schematic of the experiment set-up is provided in Figure 16. The study by Miller *et al*. (1998) found

no significant difference between the patellofemoral contact force of the native knee compared to a knee that had undergone total knee arthroplasty. This method was used on cadaver knees and is not suitable for *in vivo* testing.

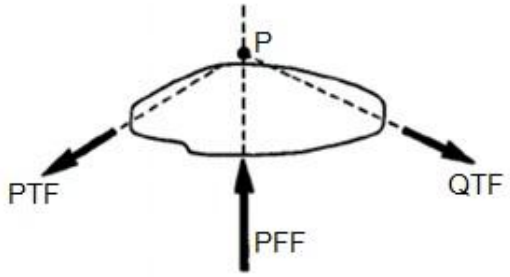

Figure 15: Representation of patellar force. PTF represents the patellar tendon force, PFF represents patellofemoral contact force, and QTF represents the quadriceps tendon force. P represents the point where a cable was attached (Miller *et al.*, 1998).

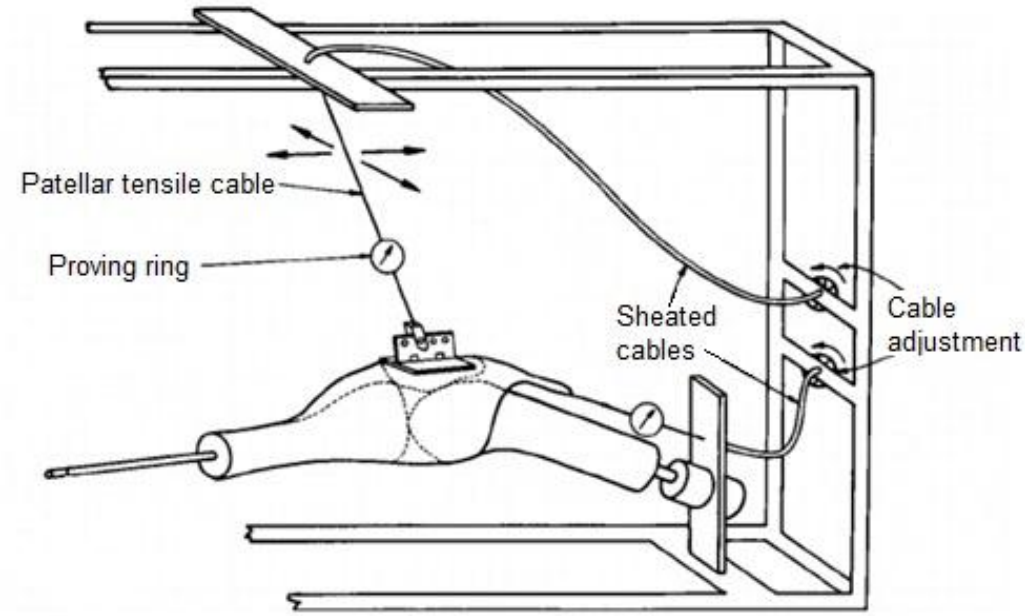

Figure 16: Experiment set-up of Miller et al. (1998).

2.6 Literature study conclusion

The knee is one of the largest joints in the human body. End-stage osteoarthritis in the knee can cause immense pain and discomfort and could even lead to disability (Vos *et al.*, 2012). The most common solution for osteoarthritis is a total knee replacement, where the bone ends of the joint are replaced with prostheses (Becker *et al.*, 2011). While this is an optimum solution, problems do arise post-surgery. These problems include anterior knee pain, which affects more than 20% of patients (Matz *et al.*, 2019). The cause of this phenomenon is not yet known.

Some research suggests that overstuffing the patellofemoral joint during surgery could be the cause of post-operative anterior knee pain (Matz *et al.*, 2019). The theory behind this suggests that thicker patellar buttons increase the amount of direct contact force experienced by the patellar button.

Researchers have attempted to gain a better understanding of the phenomenon by measuring the direct contact force of the patella, using multiple methods. These methods have side effects, such as not being repeatable and not being suitable for *in vivo* testing.

3 Design of experiment

3.1 Overview

Given the aim of the study — to directly measure the contact force experienced by the patellar button prosthesis used in total knee arthroplasty in a simulated environment — various components had to be designed and manufactured for the set-up of the experiment.

First, a force sensor had to be designed and manufactured to measure force in small spaces, such as the patellofemoral joint. The sensor had to be interrogated wirelessly, using an antenna, which was the next feature to be designed and built. To determine the effect of different patellar button thicknesses on the direct contact force of the patellar implant, these buttons had to be designed and manufactured in various thicknesses.

A test rig was designed to calibrate and test the force sensor. The test rig had to fit patellar buttons of varying thicknesses, to test their effect on the contact force. The test rig components were designed specifically to be incorporated into the Mechanical Testing System (MTS) Criterion Model 44 of the Department of Mechanical and Mechatronic Engineering at Stellenbosch University, which has a maximum loading capacity of 30 tons.

3.2 Force sensor design

Previous studies have attempted to measure direct patellofemoral contact force, but several problems existed with the methods used, rendering these approaches unusable for the present study. These problems included the process not being repeatable or the measuring devices needing to be connected to external sources, which could have caused inconsistency in the results, as the medial reticulum could not be closed fully. This also prohibited future *in vivo* verification of patellofemoral contact force. Therefore, in the present study, it was decided to use the novel force sensor technology designed by Drazan *et al.* (2018). This decision was made due to research having shown this force sensor to be small, wireless, and accurate. To recreate the sensor in the present study, research was done on its workings and manufacturing process.

Although the sensor is not a commercial product, it is patented, and redesigning the physics of the sensors was therefore not within the scope of the present study. The present study was conducted in collaboration with the Musculoskeletal Mechanics Laboratory (MsM) of the Department of Biomedical Engineering at Rensselaer Polytechnic Institute (RPI), where the technology used in the present study was applied to design different configurations of these sensors, and to enable use the technology in a new application. The manufacturing process and

materials used were adapted for the design to be appropriate for specific application in the present study. The force sensor design is based on the novel design of the passive sensors of Drazan *et al*. (2018). Specific design dimensions and materials needed were researched and given to the MsM laboratory for the physics design of the final sensors.

The size constraint of the patellofemoral joint is a limiting factor in the technologies and sensors that can be used to measure forces within the knee, as the traditional force sensors generally used are too large. This resulted in the need to design and test alternative technologies specifically aimed at this application (Dion *et al*., 2015). The force-sensing technology used in the present study was initially developed by Drazan *et al*. (2018). The technology created the opportunity to fabricate and integrate a force sensor without sacrificing the patellofemoral implant. The sensor developed by Dion *et al*. (2015) is shown in Figure 17.

Figure 17: Passive force sensor designed by Dion et al. (2015).

The sensor consists of two copper coils: one spiralling clockwise and the other anti-clockwise. Only one of these coils is visible, as they are placed parallel to one another. Between the two coils is an intervening dielectric layer with specific material properties, as illustrated in Figure 18.

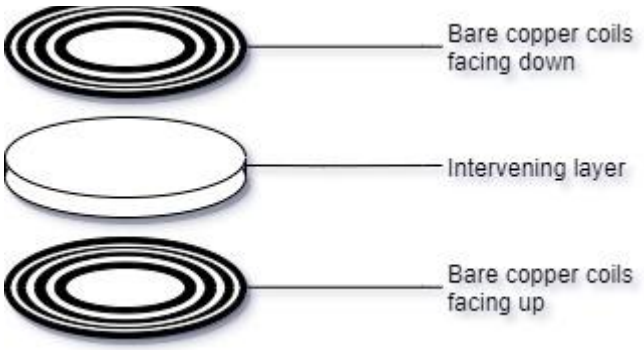

Figure 18: Assembly of two identical coils and an intervening layer to create a sensor.

Essentially, the two copper coils act as a parallel plate capacitor. The sensor's behaviour is influenced by the coil's geometry and size, as well as the physical properties of the intervening layer (Drazan *et al.*, 2018). The dielectric layer between the two coils has a certain resting thickness, which becomes smaller as the sensor experiences more force, and subsequently flattens out. The distance between the two coils has an influence on the sensor's resonating frequency, expressed in Equation (1).

$$f_{res} = \frac{1}{2\pi\sqrt{LC}} \tag{1}$$

The resonating frequency (f_{res}) is influenced by the inductance (L) and capacitance (C) of the coils. The two coils act as a capacitor, and, thus, the only variable in this equation is the capacitance; the inductance remains constant. The only variable the capacitance has is the distance between the two coils, expressed in Equation (2).

$$\Delta C = \frac{\varepsilon A_C}{\Delta l} \tag{2}$$

The change in capacitance (ΔC) is a function of the dielectric constant (ε) of the material, the area of the sensor (A_C), and the change in the distance between the two coils (Δl). Thus, if the resonating frequency of the sensor is known, the capacitance can be calculated and, therefore, also the distance between the two coils. The change in height of the intervening layer can be used to calculate the engineering strain using Equation (3)

$$e = \frac{\Delta l}{l_0} \tag{3}$$

with l_0 being the initial thickness of the intervening layer. The engineering strain (e) can then be used to calculate the stress (σ) experienced by the sensor, using Equation (4).

$$E = \frac{\sigma}{e} \tag{4}$$

In order for the engineering strain to be calculated, the Young's Modulus (E) of the material is required, which is obtained from the selected dielectric material properties tables. As the resting distance between the two coils is known, the change in distance when force is applied can be calculated using Equation (5).

$$\sigma = \frac{F}{A} \tag{5}$$

In Equation (5) the area (A) of the sensor is used to determine the force the sensor experiences (F). Thus, the material properties of the dielectric layer are crucial in determining the force the sensor is experiencing.

The resonant frequency of the sensor can be measured using an antenna and network analyser. The network analyser sends out a range of frequencies previously defined by the user and characterises the return attenuation of the frequencies. The sensor starts to resonate when placed inside the radio frequency energy emitted from the network analyser, via the antenna that is inductively coupled with the sensor. The system acts as a band reject filter at the sensor's resonant frequency. The antenna analyser continuously records the signal returned, but when the sensor absorbs all the energy, no signal is returned, and a dip is evident in the signal data. The lowest part of the dip indicates at what frequency the sensor resonated, and, thus, the resonated frequency of the sensor under the specific conditions can be determined.

Previous work done with the sensors indicated that plotting of the calibration data of the sensors results in a straight line, as a linear relationship exists throughout the range of load applied. The results of calibration of sensors done by Dion *et al*. (2015) are shown in Figure 19, where each of the three lines represents a different sensor, designed to have a different resting frequency.

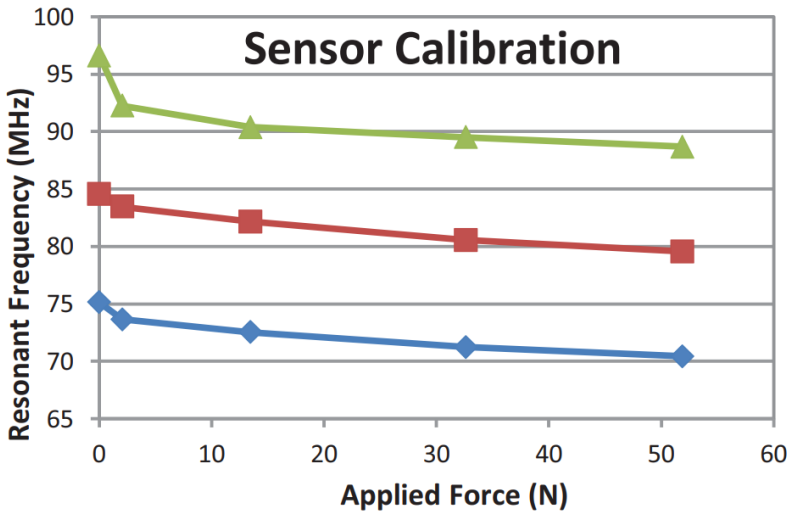

Figure 19: Sensor calibration values obtained by Dion et al. (2015).

Sensors calibrated by Drazan *et al*. (2018) showed a linear response, with an average R^2 value of 0.943 when calibrating three different sensors. Drazan *et al*. (2018) noted that increasing the load experienced by the sensor caused the resonant frequency to decrease proportionally.

The different parameters needed by the MsM laboratory to calculate the amount of turns the coils should consist of are provided in Table 1. These parameters and the thought process as why they were chosen are explained after Table 1.

Table 1: Design requirements for the force sensors needed.

Property	Value
Small force sensor inner diameter	7 mm
Small force sensor outer diameter	13 mm
Large force sensor inner diameter	31 mm
Large force sensor outer diameter	34 mm
Trace width	100 µm
Trace spacing	100 µm
Trace height	30 µm
PCB FR-4 (substrate) thickness	0.78 mm
Substrate dielectric constant	4.4
Maximum load	1 kN
Material of intervening layer	Parylene C
Intervening dielectric constant	2.95
Thickness of intervening layer	80 µm

The first design constraint of the force sensor was its shape and size. The ideal force sensor had to cover the entire surface of the patellar button, to ensure no load sharing took place. This is illustrated in Figure 20.

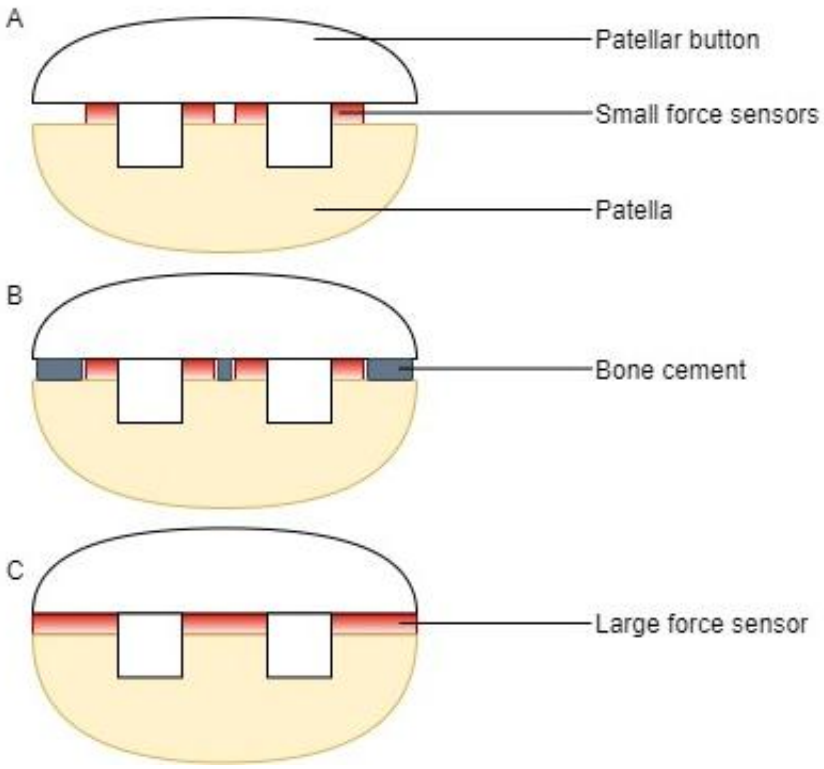

Figure 20: Part A: Smaller sensors, which create negative spaces between the patellar button and the patella, which, in turn, results in a poor fit. Part B shows the solution of adding bone cement, which stabilizes the fit, but creates load sharing. Part C shows that a large force sensor will provide both a good fit and prohibit load sharing.

As the extant research discussed in Chapter 2 suggests, the contact force area changes from proximal to distal as the knee moves through the flexion range (Horng-Haung *et al.*, 1996). Research also suggests that the patellar button moves laterally as flexion takes place (Horng-Haung *et al.*, 1996). In order to clearly see the distribution of the patellofemoral contact force in the present study, it was decided to design three small force sensors, each placed around a peg of the patellar button. Thus, the three force sensors were placed as follows: proximal, lateral distal, and medial distal. In order to place the force sensors around the pegs, the force sensors needed to have holes, which meant a halo sensor design would optimal (see Figure 21). The inner and outer diameters of the designs were calculated to fit inside the size constraint of the patellar button, which had an outer diameter of 36 mm and pins with an outer diameter of 5 mm, as shown in Appendix B. To measure the total force experienced, a large halo coil was designed to be placed around the three smaller coils, as shown in Figure 21. The inner and outer diameter were designed to fit the patellar button, as well as the three smaller force sensors around each patellar button peg.

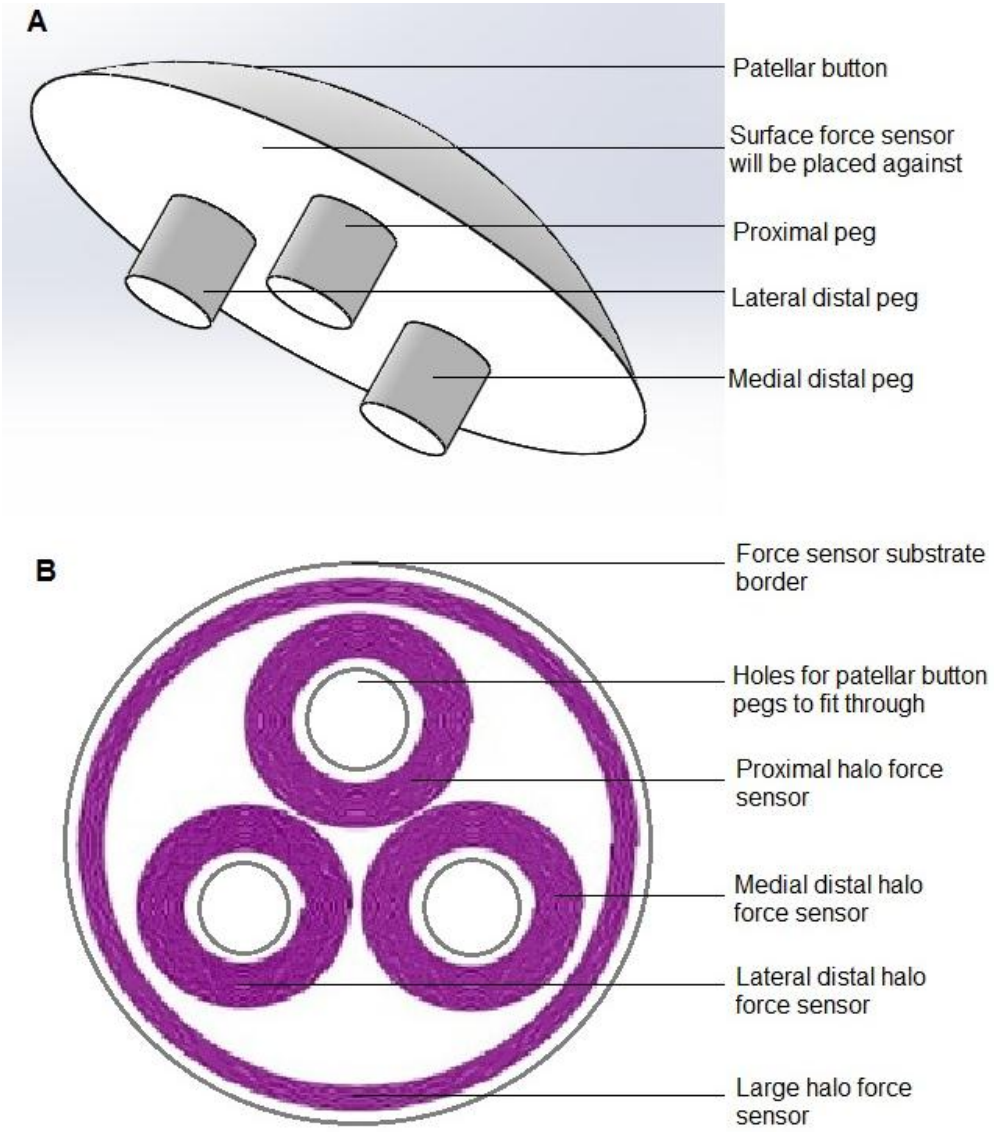

Figure 21: The four-in-one sensor designed for the present study. Three different small sensors were placed around the patellar button pins, with a large sensor surrounding them.

The manufacturer of the coils suggested that the finest possible width and thickness of the traces would be 0.1 mm, which suggestion was implemented. The standard trace height the manufacturer uses is 30 µm. Standard FR-4 PCB, which is widely available, was chosen as the substrate for the coils to be printed on, as it suited the requirements for the force sensor.

Biomedical modelling suggests that the patellofemoral reaction force during daily activities ranges between 2.5 to 7.6 times the body weight (Matz *et al.*, 2019). Therefore, ideally, the force sensor needed to measure up to 9 kN. Since the technology had not been designed for testing forces that high, but only up to 250 N,

it was decided to design the force sensor to measure forces up to 1 kN. This would show whether the sensors could be designed for larger forces for future projects, while being used to measure the effect of patellofemoral forces in a knee being bent without carrying any body weight on it, as was done in the study of Oishi *et al*. (1996), in which testing was done up to only 100 N.

The intervening dielectric layer is a crucial part of the force sensor design. The important material properties that need to be considered include the Young's modulus, the dielectric constant, and moisture absorption. A higher Young's modulus is desirable, as this ensures that a larger range of forces can be measured, while still deforming under hydrostatic pressure. A low moisture absorption rate ensures that the sensor does not short-circuit during future *in vitro* tests where body fluids are present, which could influence the results. The dielectric constant may improve the sensitivity of the force sensor, as a higher dielectric constant increases the capacitance of the force sensor. Three materials were considered for an intervening layer. Polymethyl methacrylate (PMMA), Polydimethylsiloxane (PDMS), and Parylene C.

PMMA can be spin-coated, which is a simple process that yields a thin, uniform layer. It has a high Young's modulus, which means the force sensor is able to measure a broader range of forces, but it is less sensitive to change in the force. Unfortunately, it has a very high moisture absorption rate, meaning the dielectric properties change rapidly when the force sensor comes into contact with a liquid.

PDMS can also be spin-coated, but has a lower Young's modulus, which means the force sensor is more sensitive, but will deform drastically under high loads, which is not desirable. This material has a low moisture absorption rate.

Parylene C was chosen for the present study, as it has a high Young's modulus, meaning it deflects less under large loads, and has a low moisture absorption rate, which is desirable for future *in vitro* testing where body fluids are present. Unfortunately, Parylene C can only be applied to the bare copper coil traces using a vapour deposition process, which is more complicated.

While researching extant studies that used chemical vapour deposition processes, it was found that the University of the Western Cape had a chemical vapour deposition system that could be used to coat the bare copper coils of the sensors. Unfortunately, during testing, it was found that the current used to heat the boat in which the source material was placed was too high at its lowest setting of 30 A. Therefore, the source material (Parylene C) immediately vaporized, which caused an inconsistent splatter pattern on the substrate, instead of a uniform coating. This phenomenon is shown in Figure 22.

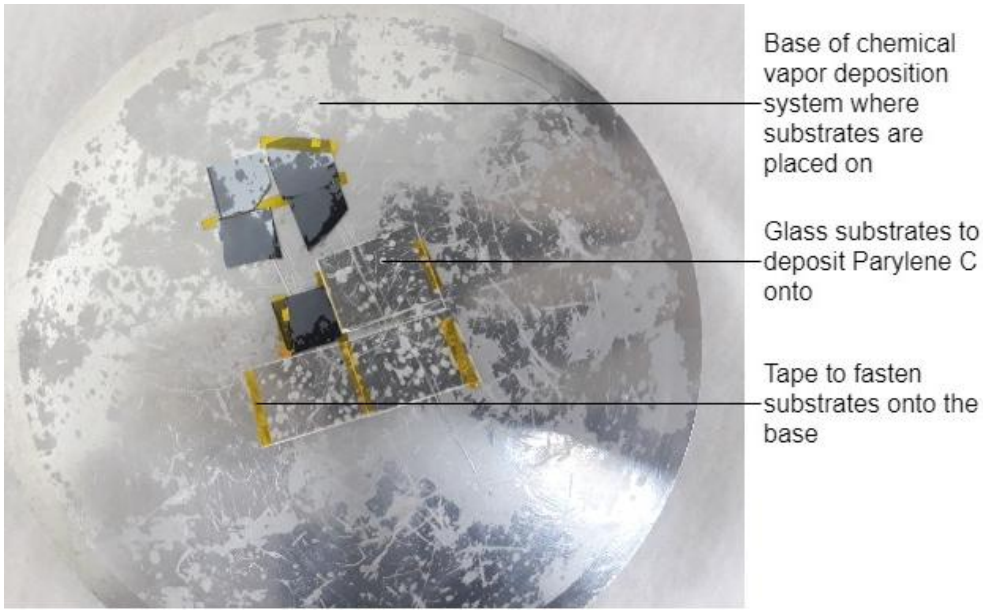

Figure 22: Inconsistent splatter pattern of Parylene C, evident in white speckles created by the chemical vapour deposition system.

A different method for the vapour deposition process was created using a ceramic tube placed inside an oven. The application of the intervening layer between the coils was done using a vapour deposition process. This was done by placing 300 mg Parylene C in a small ceramic boat and placing it in a ceramic tube, in the centre of the heating zone, ready to evaporate. The bare coil substrate was placed into a ceramic tube, 220 mm from the centre of the source boat, at a 20^0 tilt, to improve the uniformity of the thickness of the Paylene C deposit. The carrier gas was 200 standard cubic centimetres per minute (sccm) of nitrogen, which resulted in a pressure of 2 mbar inside the tube. The Parylene C, at 2 mbar, started to evaporate at 80^0 C. The temperature was increased to create a higher evaporation rate. The source temperature was increased from room temperature to 110^0 C in 15 minutes, and remained at 110^0 C for another 15 minutes to ensure all the source material evaporated. A thermocouple attached to the bottom of the substrate holder measured a maximum of 35^0 C during the deposition. The system was cooled for ten minutes with a fan, to increase the cooling rate. This process resulted in a conformal layer of the desired thickness.

Each coating was measured using a profilometer, to determine the roughness and distribution of the deposition. The thickness of the Parylene C layers was specified after experimental coating had been done to determine feasible layer thickness while maintaining even coverage of the material. The maximum thickness of the material after deposition was 40 µm. This was done with very little roughness. The thickness could not increase, even with the use of multiple layers or extending the time in the oven. Adding two of these force sensors together resulted in a total thickness of 80 µm.

A challenge that arose during preliminary tests was that the resting frequency of the force sensors did not remain constant. Further investigation showed that the coils that were only placed on top of one another would not remain in position, due to micro movements, illustrated in the exaggerated schematic in Figure 23. This led to the decision that the two layers should permanently adhere to one another.

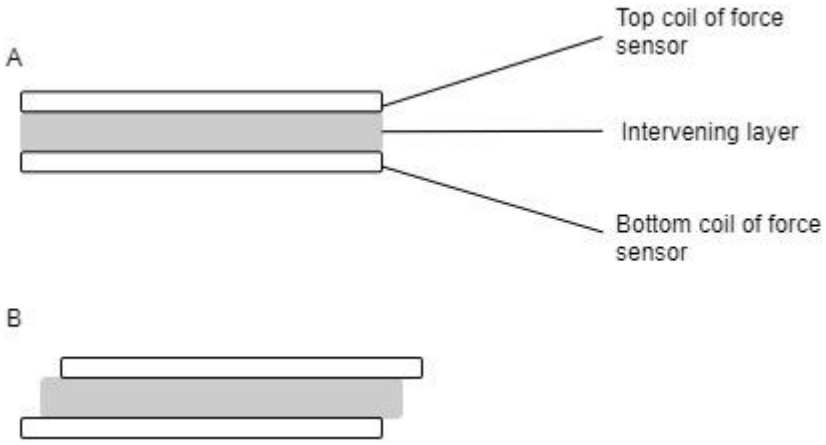

Figure 23: Part A: The desired configuration of the two coils placed directly on top of one another. Part B: An exaggeration of how these coils could move and ultimately change the properties of the sensor.

The solution was tiny holes manufactured into the coil design boards to allow the coils to be more accurately aligned and fixed. As the traces were very small, inaccuracies could occur when lining up coils that were not identical and, therefore, not a pair. The different coils were therefore designed to have different aligning hole positions, which allowed accurate pairing of the coils, as shown in Figure 24.

Different methods of adhering the two coated coils together so that no movement could take place were inspected. Adding another adhesive material to the sensors was not an option, as this could change the distance between the two coils and change the properties of the intervening layer, which could influence the rate of compression. After considering the different options, it was decided to bond the two layers of Parylene C, as the material would adhere to itself. This was done by applying heat to the Parylene C for the material to change to a liquid state. This ensured that the two layers of Parylene C became one. The Parylene C was then cooled down again, reverting to a solid state. During this process, a constant and uniform force had to be applied to the sensor, to ensure the coils remained in a constant position throughout the process. As the vapour deposition process was done in a vacuum, it was still unclear what the exact melting point of Parylene C would be under atmospheric pressure. Initially, the coils were heated to too high a temperature, resulting in the Parylene C starting to vaporize. The problem became evident when no dip in the frequency was noted during testing, although the two coils were affixed to each other. After pulling the two coils apart, it was clear that very little of the Parylene C remained. The process was repeated until the optimum heating temperature of 80^0 C was found. This was tested by measuring the

thickness of the finished sensor at different spots with an electric Vernier calliper, confirming a uniform thickness of 1.64 mm. The holes for the patellar button pins to fit through were drilled afterwards, to ensure that these were perfectly aligned.

The only requirement regarding the desired resonant frequency of the different force sensors was that the three smaller coils would differ from one another with enough significance to easily distinguish the recorded frequency drop between each force sensor.

These parameters to calculate the number of copper turns needed in each of the coils were specified in the *MATLAB* code written by Drazan *et al*. (2018). The coil specifications are provided in Table 2.

Table 2: Number of loops of which each force sensor coil needed to consist.

Force sensor type	**Number of turns of the coil**
Small coil 1	14
Small coil 2	15
Small coil 3	16
Large coil	8

Using these values along with the parameters given in Table 1, the final coil designs were modelled using *EagleCAD*, which is an *Autodesk* software package. All the coils were drawn both separately and together in the final design placement, as shown in Figure 24. This was done in order to test the force sensors individually and then compare the output results with those obtained in testing the final force sensor containing all four coils. The final *EagleCAD* design with all the separate designs is illustrated in Figure 24. A single-coil design that indicates the traces along with the aligning holes is shown in Figure 25.

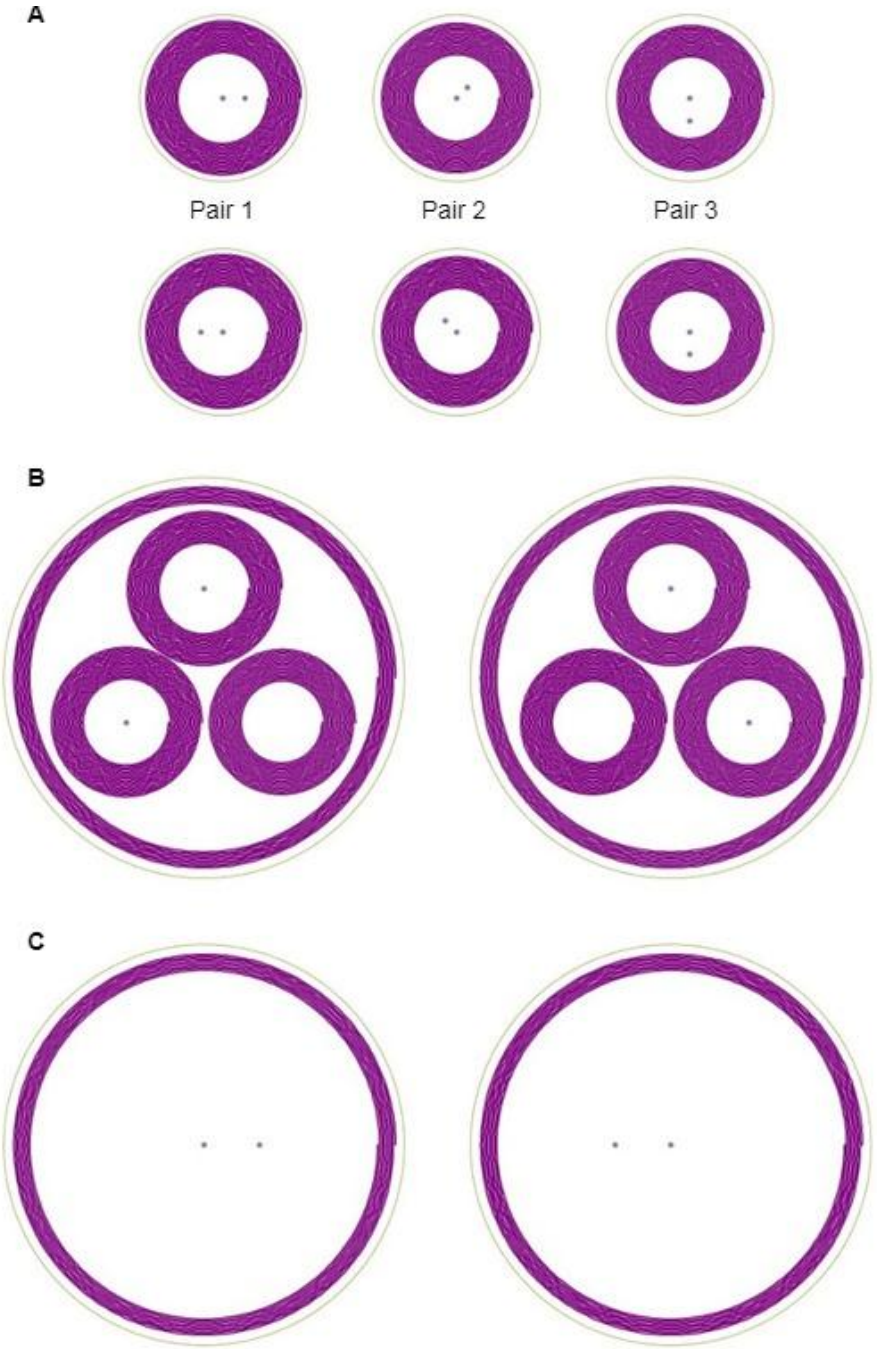

Figure 24: Part A: The three different coil designs for the three small sensors. A pair consists of identical coils that are united using the alignment holes. Part B: A pair of the final design force sensor with the four different coils together. Part C: The pair of large coil designs.

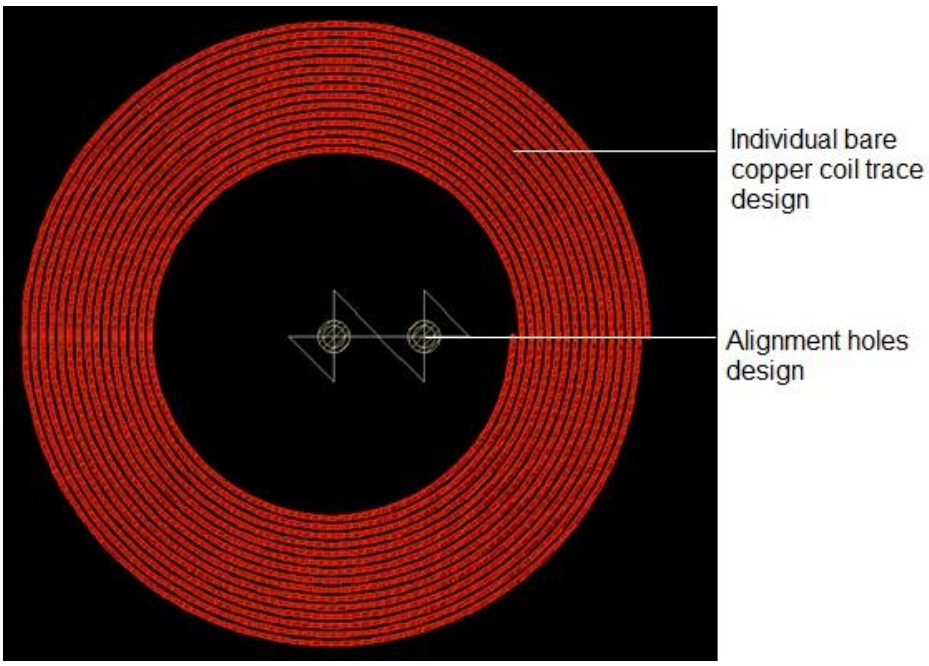

Figure 25: A single coil design showing the individual bare copper traces and the alignment holes.

After the design process, the bare copper traces were printed onto a FR-4 printed circuit board (PCB), per the manufacturer's design. Each force sensor was then cut out to the desired size, to isolate the individual coils or the group of four combined coils.

After the force sensors had been completed, another problem arose. During test-rig testing, the force sensor would be covered by a patellar button, a patellar button lid, and the belt, as shown in Figure 26, which meant the antenna placed on top of the belt would be at least 20 mm above the force sensor. For future testing in the native knee, the antenna would also need to be able to receive feedback from the force sensor from further than this distance, due to the normal biology and sizing of a knee joint. It was therefore decided that the antenna should at least be able to obtain a read range of 30 mm. During the testing of the antenna, the frequency of the small force sensors could not be read from the desired distance of 30 mm needed for the test rig, but only up to a maximum of 20 mm. Due to time constraints, it was decided not to try to improve the small force sensors or the antenna, which was an optimal design for the larger force sensor. It was therefore decided not to use the smaller force sensors for this project, and to archive the design for future research. Due to this change, the final force sensor used consisted of only the large halo force sensor surrounding all three pegs of the patellar button. The final force sensor is illustrated in Figure 27.

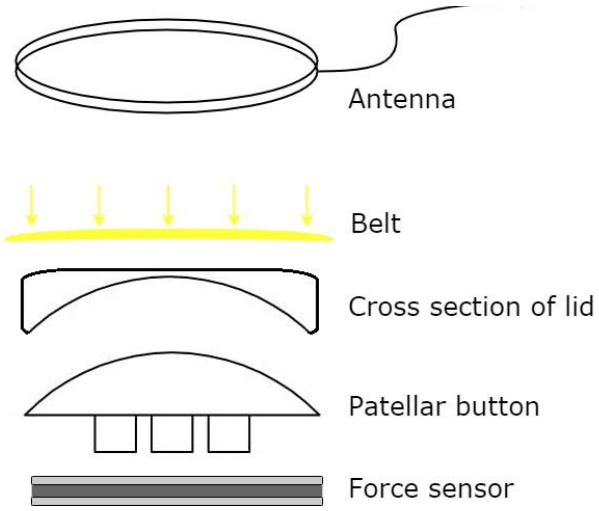

Figure 26: Assembly of the components inside the test rig, showing the distance from which the antenna needed to read the force sensor.

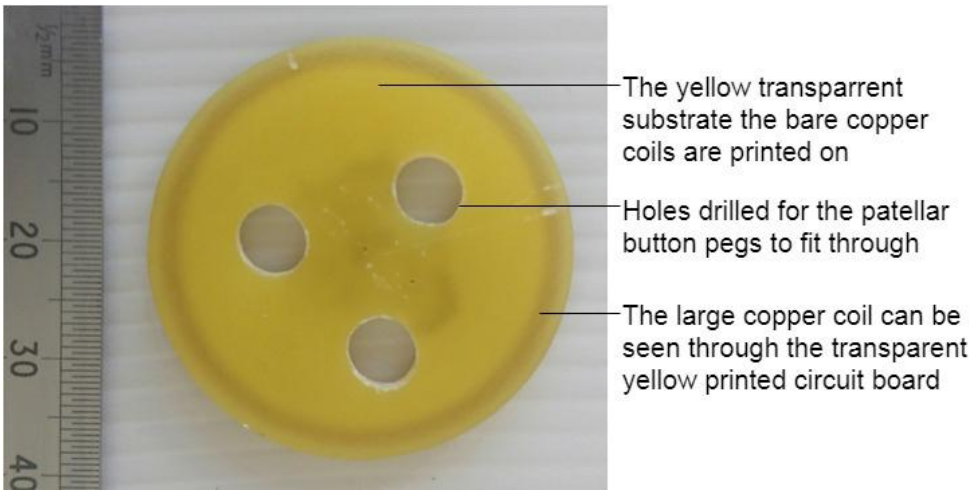

Figure 27: The final force sensor used for the experiments. A ruler is included to show the size of the force sensor in mm.

3.3 Antenna design

The force sensors communicated results wirelessly, with the use of a loop antenna. The antenna had to be designed to fit the specifications of the specific network analyser. Therefore, a 50 Ω coaxial cable with SMA connectors on both ends was used. The antenna was connected to a network analyser using an S11 parameter to send out radio frequency energy. For this project, an Anritsu 46122b network analyser was used, as it is small and portable.

The resonant frequency of the antenna was kept as far as possible from the frequency of the force sensors, so that the signal from the antenna would not influence the signal from the force sensor. It was found that fewer loops ensured that the resonant frequency of the antenna was much higher than that of the force sensors. The geometry of the antenna was designed to be similar to that of the coil; thus, a loop antenna was used. When tightly winding the wire around a PVC pipe with a desired diameter, to create more precise circles, better read range was achieved. By changing the diameter of the antenna multiple times, it was found that the optimal antenna had a diameter slightly larger than the large force sensor's outer diameter of 34 mm. This allowed for all the force sensors to be surrounded during the testing process. Smaller diameters resulted in the read range of the large force sensor being lower but did not influence the read range of the smaller force sensors. As the coils consisted of bare copper traces, copper wire was used to create the antenna. These wires were tightly wound to form the antenna, and it was therefore necessary to use insulated copper wire to avoid short-circuiting. The final design incorporated three insulated 0.5 mm copper wires, tightly wound into two 40 mm diameter loops, as can be seen in Figure 28. The antenna had a read range of 40 mm from the large force sensor, while only a 15 to 20 mm read range was achieved for the smaller force sensors.

Figure 28: The final antenna design used in the experiments. A ruler is included to show the size in mm.

3.4 Patellar button design

Custom patellar buttons were designed and manufactured for the experiments. The initial computer-aided design (CAD) models were designed to mimic the standard medium patellar button design as closely as possible (see Appendix B). Thereafter, additional designs were created from the initial design, with varying patellar button thicknesses. This was required in order to test the effect of different patellar button thicknesses on the contact force of the patella. In order to limit the effect of load sharing on the experimental procedure, a back plate was designed to fit with a standard medium-sized patellar button in all its variations. The design allowed for the force sensor to be placed between the patellar button and the back plate. The addition of a back plate would result in a change to the current surgical procedure, requiring the drilling of holes with a larger diameter.

3.4.1 Patellar button design

With a three-dimensional scan of a standard medium-sized patellar button, the 3D rendering of the object was used as a basis for the patellar button design. The design was then redrawn using *SolidWorks*, to create the initial base patellar button model. The model was then used as a base from which to create the different patellar buttons. As this project focused on the effect that different patellar button

thicknesses have on the amount of force experienced on the patella, the only variable that changed in the initial patellar button model was the thickness of the button. Six different patellar buttons of varying thicknesses were made, the first of which was the standard thickness. The original patellar button thickness is shown on the left of Figure 29. Only the thickness of the dome was changed, while the curve diameter of the dome and the length of the original pins were kept constant. In each iteration, the patellar button thickness was increased by 1 mm. Thus, the thickest button was 5 mm thicker than the standard button. These buttons were 3D-printed using PLA filament with as large an infill as possible, to avoid material voids.

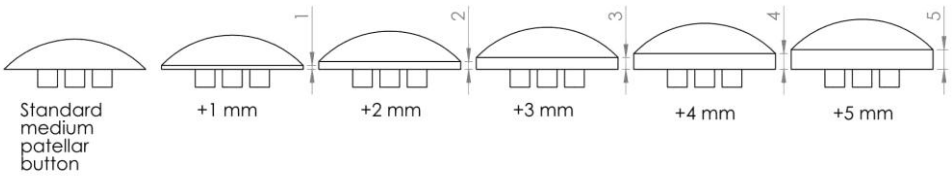

Figure 29: The custom patellar buttons designed. Starting (on the left side) is the standard medium-sized button, followed by buttons of increasing thickness with each iteration (towards the right) by 1 mm, with the last iteration (on the right side), with a thickness increase of 5 mm.

3.4.2 Design of back plate

Back plates for the patellar buttons were designed to ensure that no load sharing occurred around the force sensor due to bone cement, large gaps, or any other factors. These backplates ensured that all the force experienced by the patellar button was measured by the force sensor, as shown in Figure 30. As shown in Figure 31, the back plate was designed to be modular with the standard medium patellar button model. The back plate fit snugly into the patellar button on one side, and into the native patella on the other. The force sensor was intended to fit between the button and back plate, to ensure that no load sharing took place over the force sensor. The back plate could still be cemented into the native patella if the surgeon so prefers.

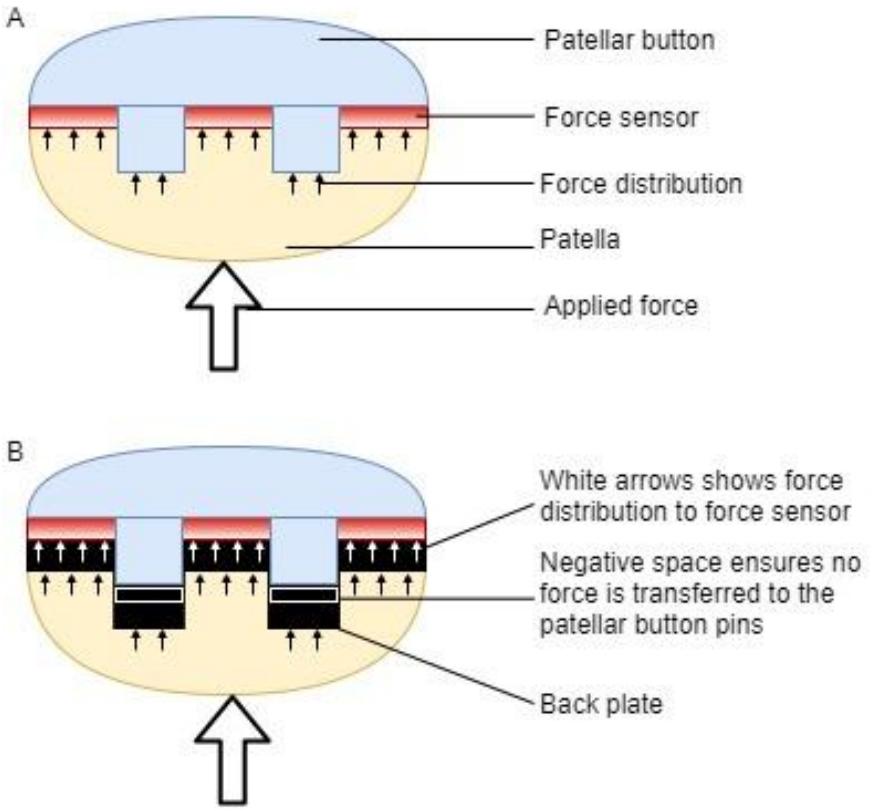

Figure 30: Part A: Force distribution without a back plate. The force is divided between the patellar button and the force sensor. Part B: Exaggerated back plate. Due to a negative space created between the back plate and patellar button, the force sensor measured the entire force.

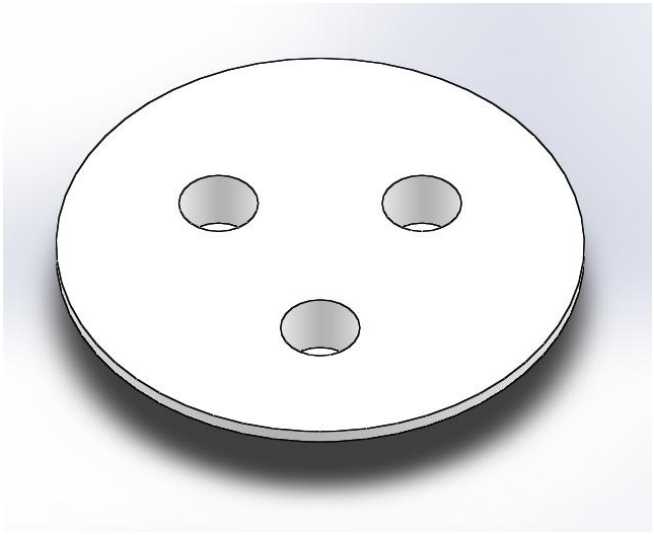

Figure 31: The back plate designed to fit onto the patellar button so that no load sharing occurred over the force sensor.

3.5 Design of test rig

A mechanical test rig system was designed to test the different patellar buttons. The original idea behind the test rig was to mimic the natural knee. The components of the knee were analysed to decide which components should be incorporated into the test rig design. A simplified figure of the knee showing the elements needed for the test rig is provided in Figure 32.

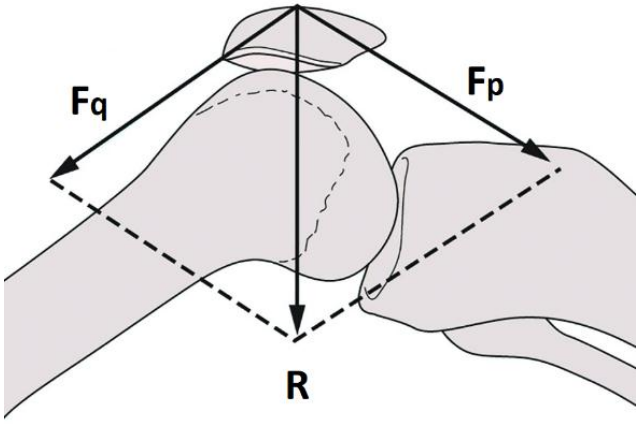

Figure 32: A representation of the forces influencing the patellofemoral contact force. F_q represents the quadriceps force, F_p represents the patellar ligament force, and R represents the reaction force (Loudon, 2016).

As the area above the patella is small, it would be difficult to attach two different elements to represent the quadriceps force and the patellar ligament force. Instead, it was decided to have a belt cover the patella and applying force from both sides. To create controlled tension in the belt, a mechanical testing system (MTS) was incorporated into the design. The MTS also ensured that all experiments were easily repeatable. To ensure that the angle between the quadriceps force and the patellar ligament force was kept constant, the belt needed to be in a fixed position when adding the tension. This would also give valuable information to do tests at various knee-flexion degrees. In such testing, tension should be added to both sides of the belt, and the rig should also be fastened to the MTS. Thus, the best solution was to fasten the test rig to one of the attachment points of the MTS, while the other attachment point of the MTS added tension to the belt. Therefore, the rig was designed with the knee in a horizontal position, as shown in Figure 32. With this configuration, the two sides of the belt could be pulled from the same direction. To ensure the two ends of the belt joined together and that accurate angles were created over the patella, pulleys were incorporated into the system. The pulleys changing the direction of the force ensured that no moment existed, which is important, as an MTS cannot accommodate moments.

Once the design and the specific MTS that would be used was known, it was decided that the pulleys take up too much space in the design, and that the desired angles could not be obtained. Instead of using pulleys, the pins that would attach the pulleys to the test rig were instead only fastened with circlips, so that they could rotate freely and act as pulleys. To strengthen the test rig, it was decided to rather weld the pins onto the test rig than have them rotate freely.

The next problem was to ensure that the force sensor was giving the correct readings. A load cell was added to the design and placed directly underneath the patella position. This could then also be used to calibrate the force sensors.

In testing, the belt mimicking the quadriceps and patellar ligament force should be attached to the MTS, to apply controlled tension. Initially, a circular belt was chosen, but once the pins had been welded onto the rig, the belt would no longer work, as there would be no way to add or remove the belt from the system, which would be required to change the angle of the forces experienced by the patella. To change the angle the belt creates, it should be moved from one set of pins to another. To solve this, the belt was no longer circular, but straight, with loops at the ends, to fit into a D-shackle that would connect it to the MTS. Unfortunately, once testing started, the belt rotated and twisted. In the final design, it was ensured that the belt could no longer rotate, but remained in a constant flat position, by fastening it to a flat bar with bolts that connect to the MTS.

Once a suitable load cell had been found to compare the force sensor results to, the force sensor plate and lid could be designed and incorporated into the rig design. As the force sensor was to be placed between the patellar button and backplate, the lid and plate had to be designed to accommodate these shapes. To ensure a uniform force was applied to the patellar button, the lid was designed to perfectly fit the dome shape. The dome shape was machined using a computer numerical control (CNC) system. The final experiment test-rig design assembly is illustrated in Figure 33.

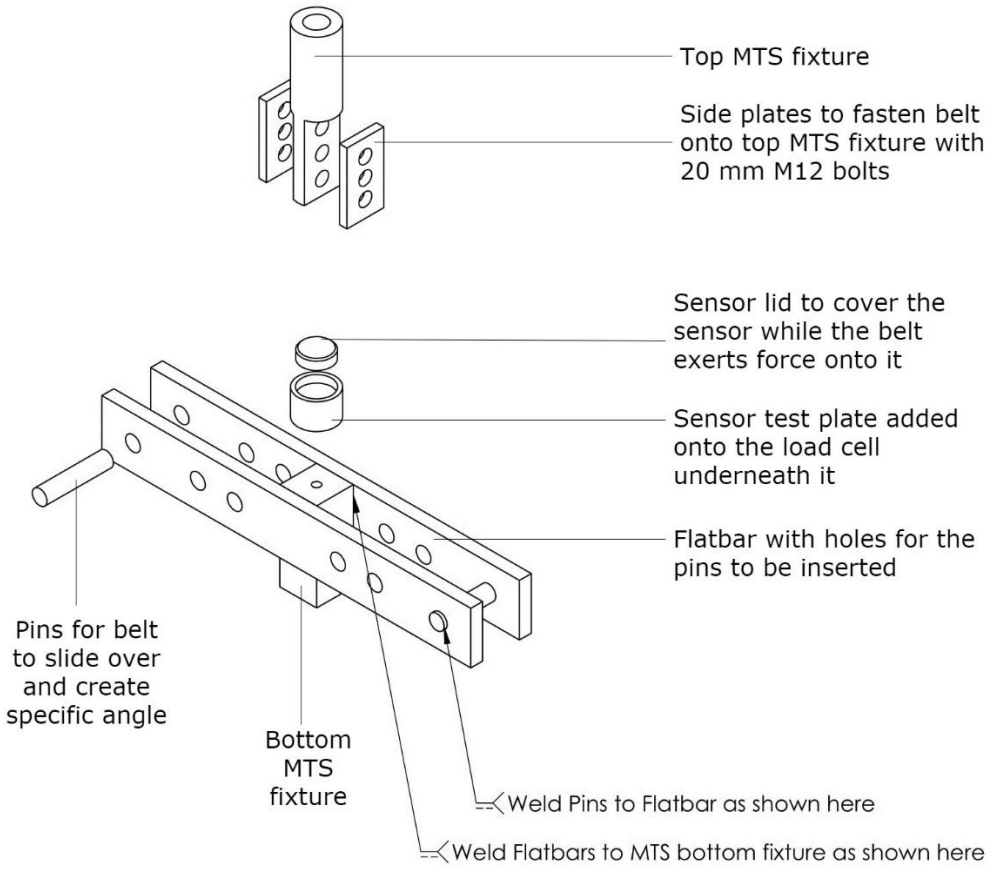

Figure 33: The CAD test-rig design showing how all the manufactured components fit together.

As shown in Figure 33, the base component connected directly to the MTS at the square bar protruding from the bottom of the base. The bottom MTS fixture was manufactured from a solid 50 x 50 mm mild steel block, tapped with a M30 hole, which ensured a firm and safe connection with the MTS. It also had an M12 tapped hole on the opposite end of the bar, in order to securely connect the load cell to the component. Two 16 mm flat bars were welded to the square bar on both sides, at identical positions, to ensure the plates were parallel to each other. The flat bars were designed with multiple holes to be drilled at corresponding positions, where pins with a 20 mm diameter would be inserted and welded into place. These pins were designed to be placed strategically, allowing for experiments with forces exerted at different angles.

The pins were designed to allow for a belt to slide over the pins, covering the force sensor or patellar button, and thus exerting force onto the force sensor during testing. The use of alternative sets of pins allowed for force to be exerted at either a 60^0, 90^0, or 120^0 angle, mimicking angles of the native knee. The components were designed with high safety factors, so that they could withstand more force than required for testing. This was done to ensure that the rig was strong enough

to withstand any unexpected or excessive forces, and that it would not deform during testing and thus potentially corrupt the results, and to ensure the safety of the test rig. Figure 34 is a representation of the 120^0 angle made by the belt, Figure 35 is a representation of the 90^0 angle, and Figure 36 is a representation of the 60^0 angle.

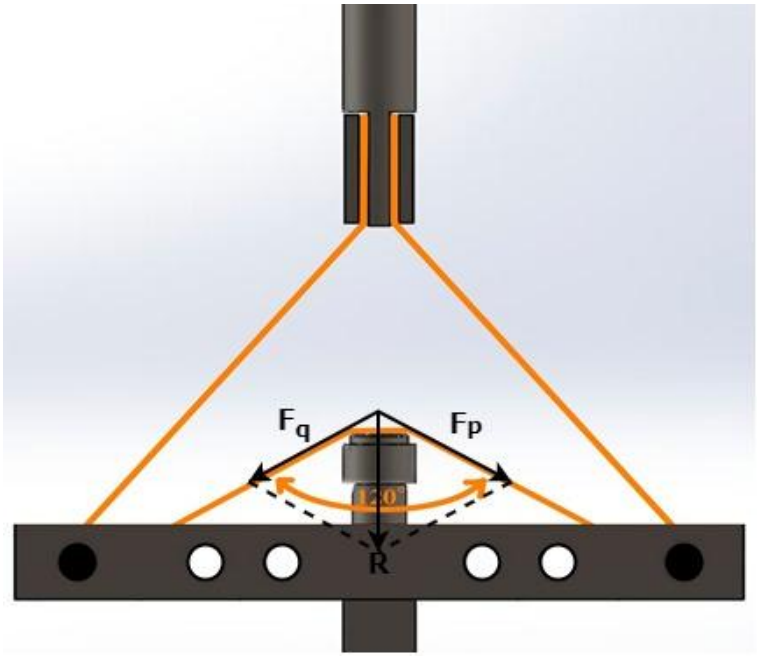

Figure 34: The test rig at a 120^0 angle, showing the recreation of the simplified forces present at the patella. F_q represents the quadriceps force, F_p represents the patellar ligament force, and R represents the reaction force.

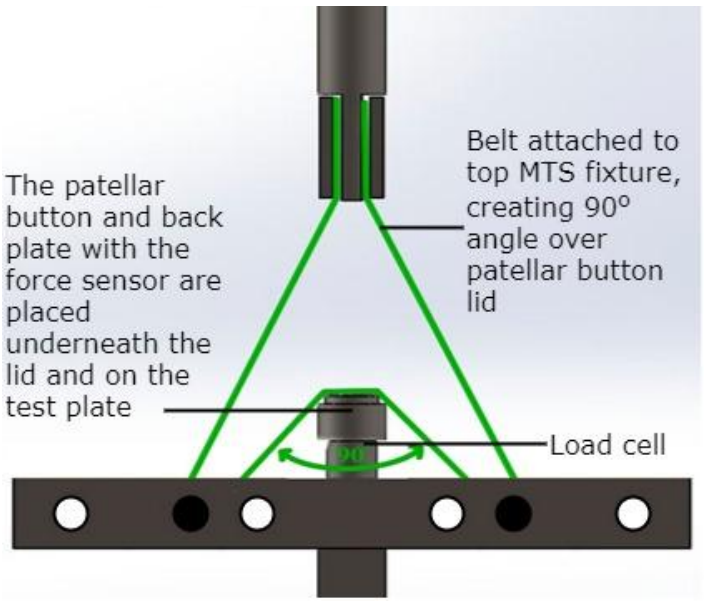

Figure 35: The test rig at a 90 ^{0} angle.

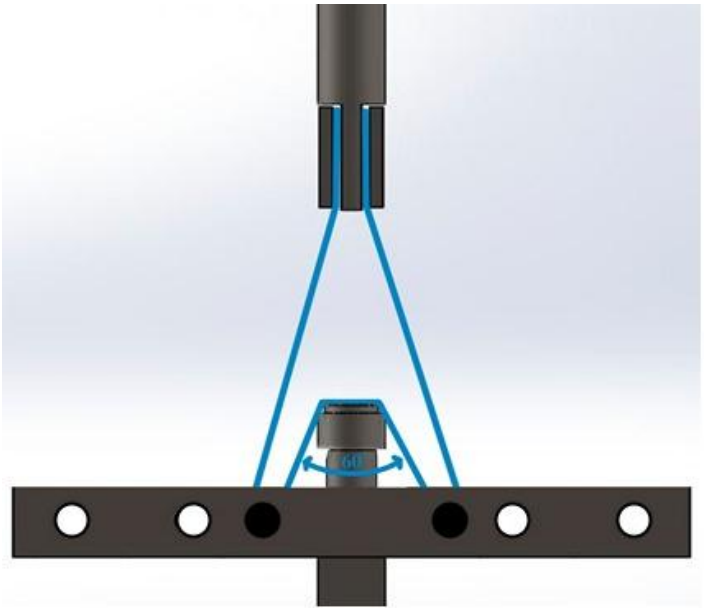

Figure 36: The test rig at a 60 ^{0} angle.

The base was designed to be connected to a load cell (see Appendix C), placed directly under the test plate for the force sensor or patellar button, as shown in Figure 35. The load cell was connected to an HBM Spider 8, which was linked to a computer, to record the data. The force sensor or patellar button was placed onto the test plate, which was manufactured from PVC to ensure the magnetic fields of the force sensor were not disrupted during testing. Two different test plates were designed. The first test plate was designed with a flat surface, allowing for only the force sensor to be tested as a control test for calibration purposes. The second test

plate was designed with three evenly spaced holes for the back plate's three protrusions to securely fit into, for testing of the entire patellar implant sensor assembly. The force sensor or patellar button was then covered with a lid that fit into the test plate. Different lids were made for different tests. For the testing of the force sensors, flat lids were used to cover the entire surface of the force sensor, in order to place a uniform force onto the force sensor. For the testing of the patellar button, the lid incorporated a dome shape designed to fit perfectly onto the patellar dome.

Additional force sensor lids were manufactured to cover only half of the force sensor or patellar button respectively, in order to exert force onto half of the force sensor or the patellar button. The purpose of this design choice was to test the force sensor and patellar button when asymmetrical forces were present. This ensured that the two layers of the force sensors stayed parallel to one another and still measured the forces correctly, even when asymmetrical forces were present. The expected problem is explained in Figure 37.

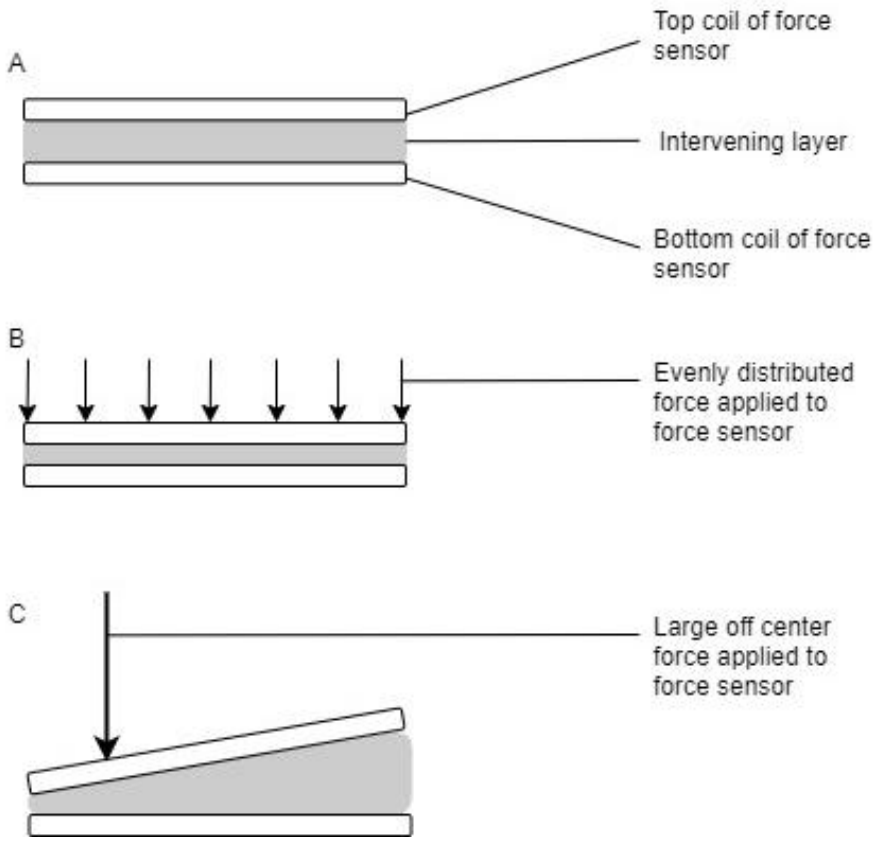

Figure 37: Part A: The force sensor with no external force present. Part B: The intervening layer flattening evenly when a force is distributed. Part C: An exaggeration of what might happen when an uneven force is applied.

These lids were 3D-printed using PLA. The prints were done with as high an infill as practically possible. The lid was then covered with a belt that translated the force applied by the MTS to the lid and, subsequently, the force sensor and load cell. To be able to mimic different flexion angles of the knee, the belt was assembled through pins on the base plate, on either side of the patella implant sensor, and then attached to the top attachment of the MTS.

The final component of the experiment test rig was the top fixture of the rig, shown in Figure 33. The fixture was designed with a 50 mm diameter and manufactured from round bar mild steal. The bar was tapped with an M30 hole to allow for connection to the existing MTS. The lower half of the round bar was milled to create a 15 mm flat surface plate to which the belt could be fastened. The bar also included three holes where M16 bolts could be inserted to tightly secure the belt on either end. Two flat bars were designed and manufactured with M16 holes spaced identically to those on the top fixture. This was to hold the belt securely between the flat bars and the top fixture on both sides, and then tightly fasten them with the M16 bolts, as shown in Figure 38.

All the individual designs can be seen in Appendix A.

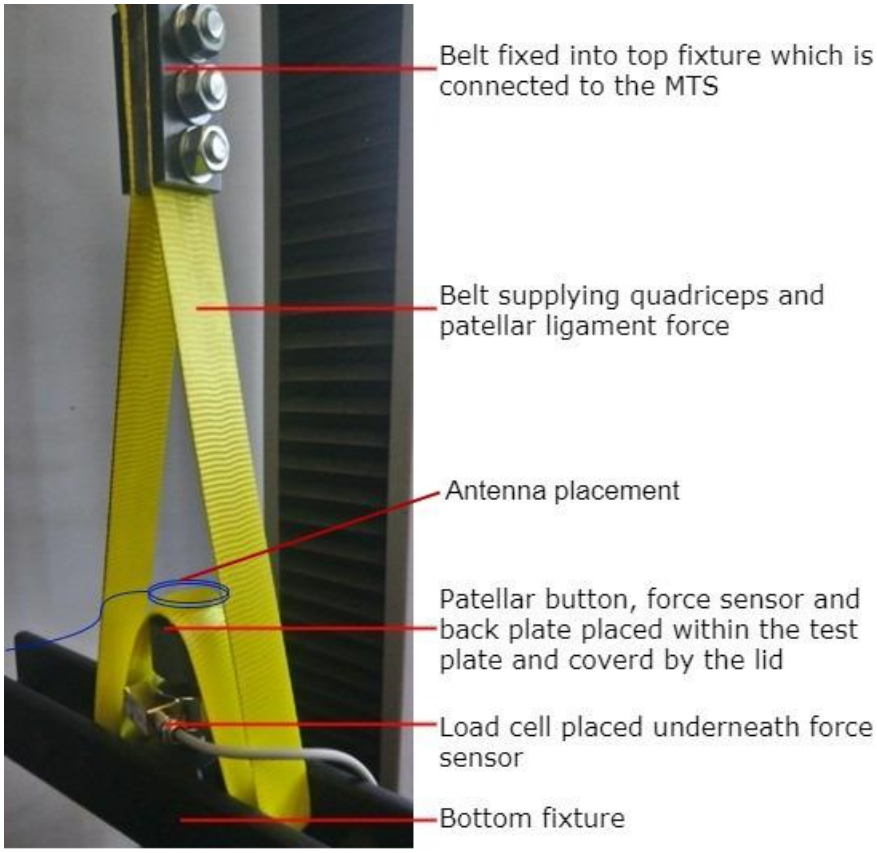

Figure 38: The test rig set up at 60 ^{0}.

The designed and manufactured test rig was set up by fastening the main section of the rig to the bottom fixture of the MTS, with the belt attachment components attached to the top fixture. The MTS allowed for the top fixture to remain stationary throughout the experiments, while the bottom fixture was moved in the vertical direction as required, to tighten or loosen the belt. This allowed the force applied to the force sensor to be variable for experimental testing. The force sensor was placed on top of the force sensor plate and covered by the force sensor lid. The lid was then covered with the belt, which was wound through the pins to form the individual angles, and then attached to the top fixture of the test rig. The belt was tightened by lowering the bottom fixture until just before the belt was under tension and no load (0 N) was recorded by the load cell beneath the force senor. This MTS position was recorded and noted as the starting state for all experimental tests at the specific angle.

3.6 Data analysis algorithm

MATLAB code was written to analyse the data obtained from the experiments. The input values obtained from the experiments were: the force measured by the MTS (which represented the tension in the belt), the force measured by the load cell underneath the force sensor, and the frequencies obtained by the force sensor. At each interval, the measurements of the load cell underneath the force sensor, as well as the frequency of the force sensor, were taken. The first part of the code created a characteristic curve for the force sensor by comparing the load cell values to the frequency values. This was done by plotting the frequency of the force sensor against the force the load cell underneath the force sensor experienced, and creating a function that best fit this data. The function was then used to calculate the force experienced by the force sensor, by entering the frequency at which the force sensor resonated in that specific moment. The accuracy of this function was also calculated by comparing all the data collected for each of the tests. The code also calculated the correlation coefficient and the goodness of the fit of the data (see Appendix D).

4 Set-up of experiment

The experiments were conducted in two separate testing sets. In the first testing set, the force sensor went through preliminary testing and validation. After a working force sensor was established with a calibration curve, the second set of experiments was conducted with the patellar buttons.

4.1 Validation of design of force sensor

Preliminary experimental testing was performed to validate the performance of the manufactured force sensor. The network analyser was set up and calibrated to ensure accurate frequency readings. The system was initially calibrated over a large range of frequencies. The ranges of frequencies at which the force sensor was expected to resonate were estimated. It was then necessary to do preliminary testing of these frequencies, in order to further reduce the frequency range emitted by the network analyser, allowing for the system to be more accurately calibrated for this region. The smaller frequency range ensured more accurate results. The antenna was then placed on top of the sensor lid covered by the belt.

The frequency of the force sensor was read by using the grid dip method. As explained in Subsection 3.2, the resonating frequency of the force sensor could be seen at the lowest point of the dip as shown by the network analyser. These values could not be recorded automatically by the network analyser, and the measurements for each test therefore had to be recorded manually. Figure 39 provides a screenshot of the grid dip results during experimentation. A marker was used to track the frequency at the lowest point in the dip.

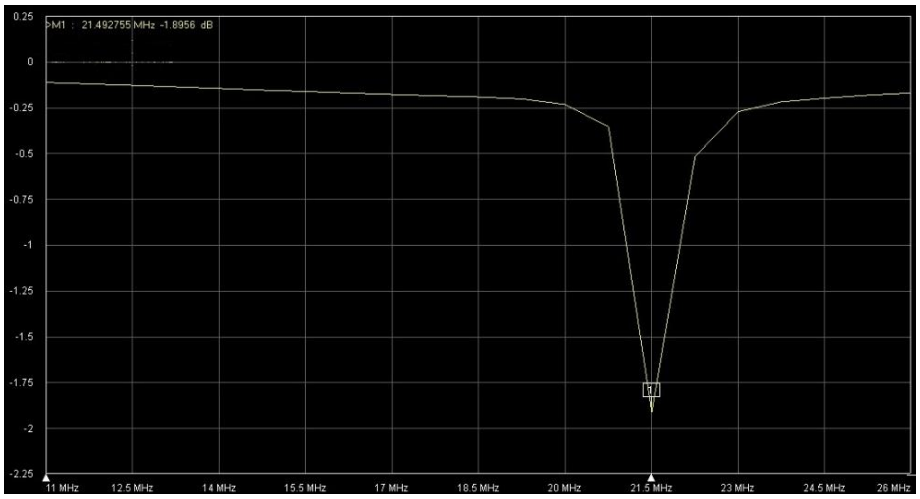

Figure 39: A screenshot of the grid dip seen on the network analyser when the antenna was placed over the sensor.

The frequency of the force sensor was measured at the starting point. The bottom fixture was then lowered in small increments, and the force was noted at every stop, together with the resonating frequency of the force sensor as measured by the antenna. The process continued until the load cell measured a maximum force of 200 N. Although the initial procedure was aimed at testing up to a maximum of 1 kN, no difference was noted after 200 N, and it was decided to cease experimentation at this point. The bottom fixture was then lifted again, until the load cell measured 0 N. This process was repeated six times, to ensure accuracy of the testing procedure and results of the experiments. The values obtained were then plugged into the *MATLAB* code. The code provided a calibration curve function, describing the relationship between the load cell and the force sensor, which was used to convert the frequency measured into the force experienced for use the tests to follow.

4.2 Patellar button tests

Once the force sensor had been validated and a calibration curve established, the patellar button tests could take place. The validated force sensor was then used (together with the test rig) to measure the direct contact force for each thickness iteration of the patellar buttons, at each of the predetermined knee flexion angles. The same procedure applied for the antenna and network analyser during validation of the force sensor was used here.

The setup of the test rig was done in a similar manner as for validation of the force sensor, with a few differences. The test rig was equipped with the patellar button test plate, instead of the force sensor test plate, and the domed patellar button lid was used, instead of the flat surface sensor lid. The patellar back plate was placed on the button test plate, and the force sensor was inserted in-between. Each of the six the patellar buttons were tested three times: at the 60^0, 90^0, and 120^0 angle.

5 Results

This chapter documents the observations made during testing, the results of the testing of the force sensor's accuracy, and the results of the effect of different patellar button thicknesses on the direct contact force experienced by the patellar button. The findings are discussed in greater detail in Chapter 6.

5.1 Force sensor test results

The network analyser was calibrated to sweep a range of frequencies between 11 MHz and 25 MHz. The network analyser provided the frequencies up to six decimals. In the no-load state, the sensor output resulted in a frequency of 21.492755 MHz. As shown by the graph of the force sensor's frequency, plotted against the load cell data of the initial six tests (see Figure 40), the change in frequency was not linear with the change of force.

The data from the six initial calibration tests were used to create a best-fit function through all the points. The best-fit line (shown in Figure 40) was used to calculate the force the force sensor was experiencing at a specific frequency. The function's R^2 value (which represented the goodness of the fit) was 0.9798, indicating that the function fit the data well.

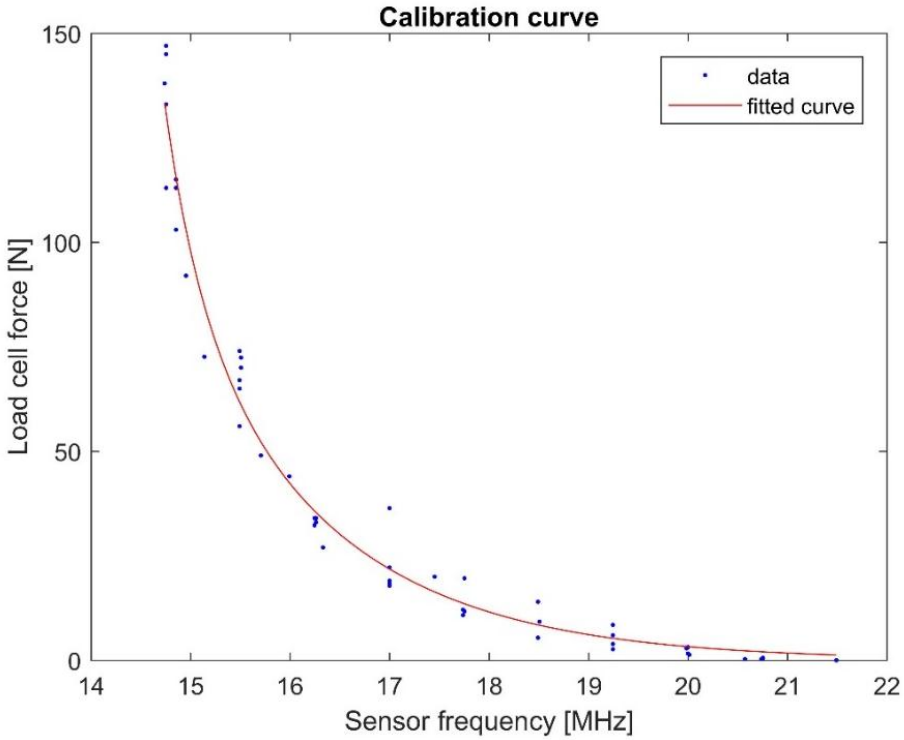

Figure 40: The best fit curve for the force sensor calibration data is shown in red.

An exponential curve was the best fit to the data as described by Equation 6. The force the force sensor experienced (F) was calculated using the frequency of the force sensor (f) in MHz:

$$F = a + bc^f \tag{6}$$

Table 3: The parameter values of Equation 6.

a	0.756797412
b	10304538.26
c	0.461289543

Using the function of the calibration curve, the calibration data's frequencies were converted to the force experienced and plotted against the force experienced by the load cell. This graph is provided in Figure 41, showing an R^2 value of 0.9802, a correlation coefficient of 0.99, and a mean square error of 22.454.

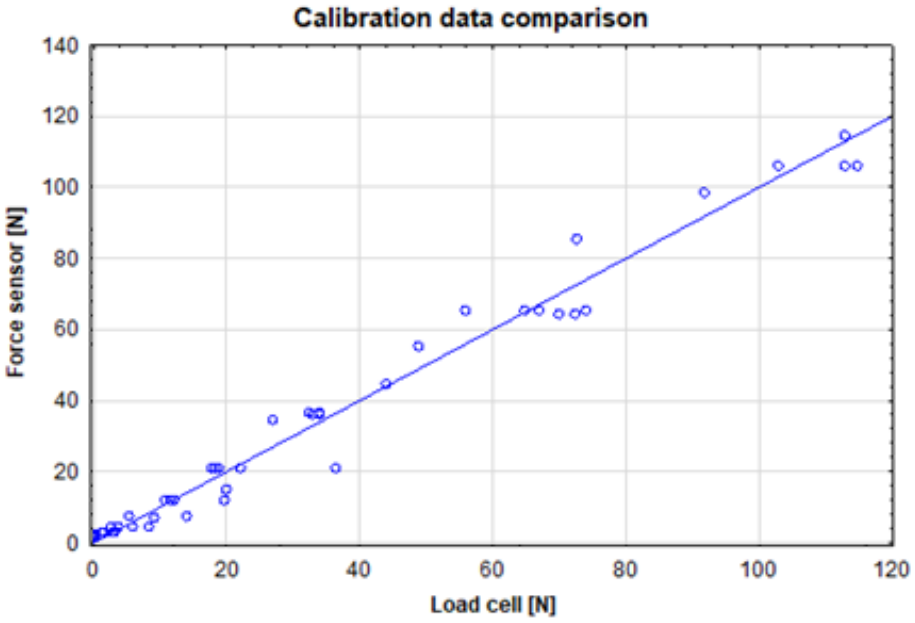

Figure 41: A comparison of the test data recorded by the force sensor and the load cell.

For the three patellar button tests, the load cell underneath the force sensor was still present. This testing was done to calculate the accuracy of the force sensor throughout the tests. The force sensor's frequency was inserted into the calibration function, to calculate the force measured by the force sensor. The force

experienced by the force sensor was plotted against the force the load cell experienced, shown in Figure 42. A best-fit line was added to the data (see Figure 42). The goodness of the fit was 0.9255, and the correlation coefficient of the data was 0.9620. The mean square error was 90.6, indicating that the force sensor's data were inaccurate.

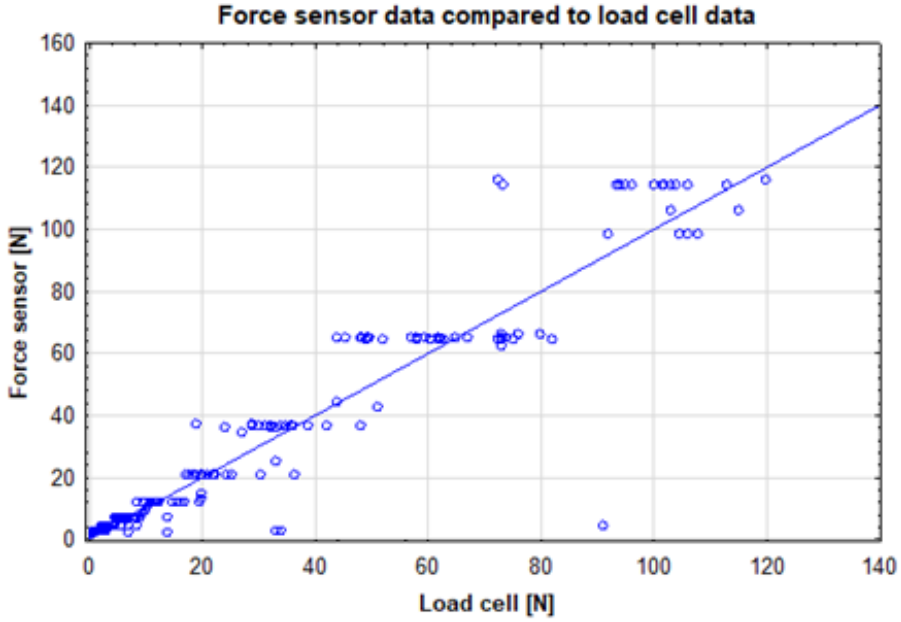

Figure 42: Test data obtained for the load cell, plotted against the force sensor data, to test the accuracy of the force sensor.

5.2 Patellar button test results

The data obtained from the force sensor were considered inaccurate, as the error margin was too large. It was then decided to use the data obtained from the load cell underneath the force sensor to compare the results of the different patellar button thicknesses.

The results of the force experienced by each patellar button was plotted against the amount of force applied to the belt at the same time for each repetition, at each belt angle. This gave the simulated relationship between the direct contact force experienced by the patellar button and the amount of force the quadriceps muscle would exert. Using these plots, repetition could then be compared, and the different buttons could be compared with reference to the same angle. An average line between the three repetitions was plotted, to calculate the slope of each patellar button at each angle at which the tests were done. One of the plotted slopes is given as an example in Figure 43.

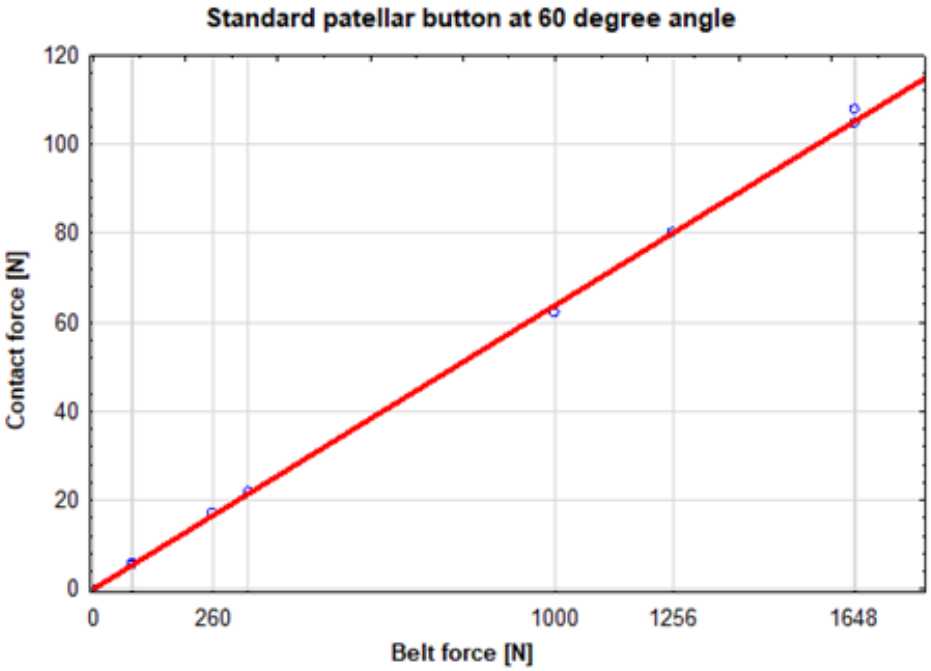

Figure 43: The slope created by plotting the values obtained by the load cell underneath the force sensor against the values obtained by the MTS for the standard patellar button at the 60 ^{0} angle.

In Figure 44, the average slope of each patellar button at every knee flexion angle is compared with vertical bars denoting 0.95 confidence intervals. The difference between the standard patellar button and the thickest patellar button was statistically significant within a 95% confidence interval at certain angles.

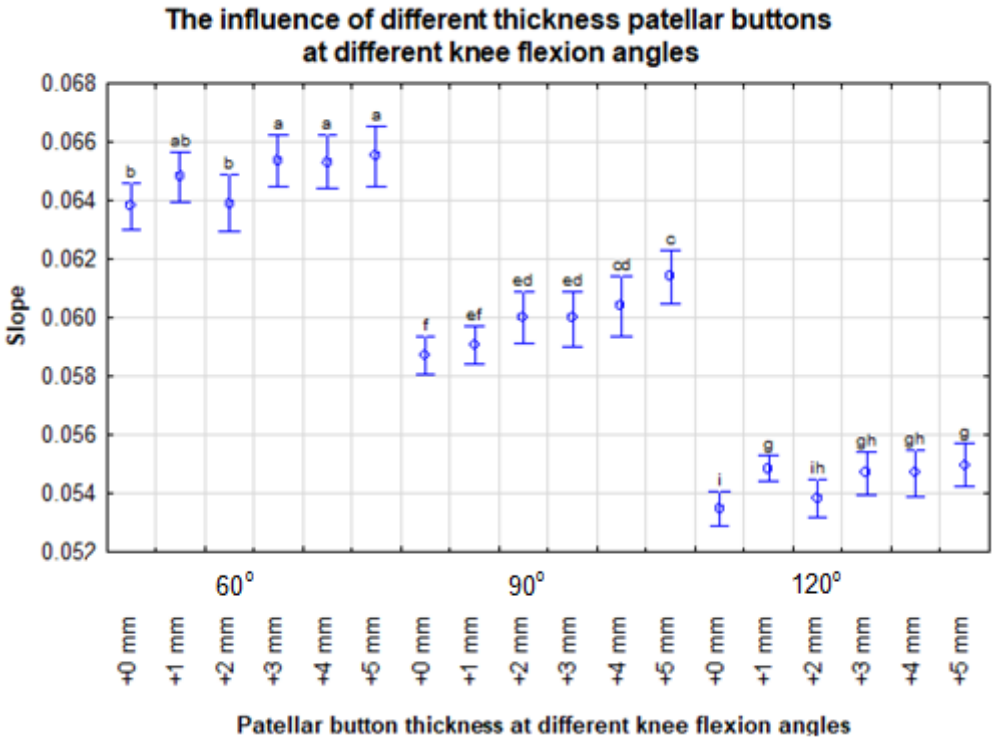

Figure 44: Comparison of the slope of each of the patellar buttons of different thicknesses at each flexion angle.

The average slope of each patellar button was taken across the different angles and plotted (see Figure 45). The overall statistical significance was $p = 0.03$, meaning that the patellar buttons of different thicknesses indeed have a significant effect on the contact force experienced by the patellofemoral joint through the full range of motion that the native knee experiences. The overall statistical significance between the different angles was $p = 0.01$, meaning that the knee angle also has a significant effect on the amount of force experienced by the patellar button.

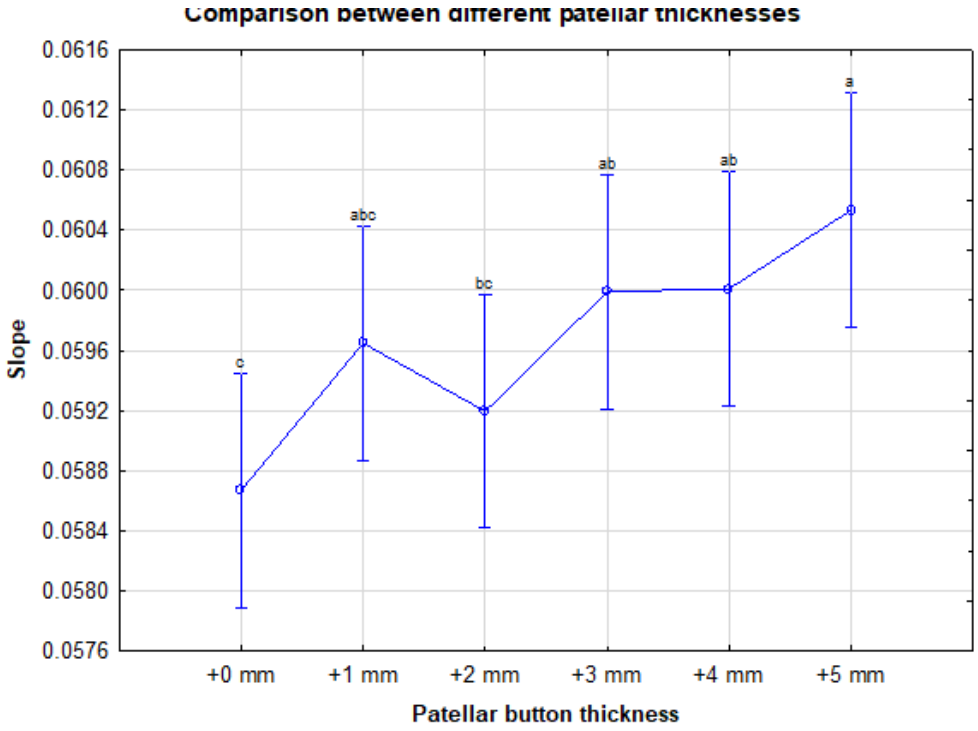

Figure 45: Comparison of the results of the patellar buttons of different thicknesses.

6 Discussion

This section provides a more detailed discussion of the results, a reconciliation of the research objectives, and recommendations for future research.

Research Objective 1 was achieved through the design of different configurations of an existing force sensor, in order to directly measure the patellofemoral contact for experienced by the patellar button prosthesis.

With regard to the force sensor calibration (Research Objective 2), a linear relationship was expected between the change in frequency and the change in force measured, as discussed in Subsection 3.2. Although Dion *et al*. (2015) found a linear relationship, the graph in Figure 19 appears to be more sensitive within the first 5 N, which correlates with the results of the present study (see Figure 40). It is also possible that if the *y*-axis were reduced to only 10MHz, one might see more of a curve, rather than a straight line.

While the calibration did not show a linear relationship, the results showed a strong correlation between the force sensor data and the load cell. However, the force sensor was not considered accurate enough for this project, given that the correlation coefficient was less than 0.99, the goodness-of-fit value was lower than 0.95, and the mean square error was 90.6. Therefore, it was decided to continue the project using the values obtained from the load cell placed directly beneath the force sensor.

The Parylene C coating process (the application of the dielectric layer between the coils) did not result in the desired smoothness, yielding a roughness of 10 µm. This could have resulted in some gaps in the intervening layer of the force sensor, which could have led to the inaccuracy of the force sensor. The aim was to use the force sensor to measure up to 1 kN, but this was not achieved, as the force sensor was only able to measure up to 120 N. Recommendations future research on improvements of force sensors include finding a more suitable method to deposit the intervening layer, to reduce its roughness. Future research could also be done on allowing the force sensor to measure larger forces by using a thicker intervening layer or a more suitable deposition method to increase the thickness of the intervening layer deposition.

Research Objective 3 was achieved through the design of a test rig to measure the contact forces experienced by the patellar buttons of different thicknesses. When the first force of 10 N was applied directly to the force sensor, the frequency changed significantly during each small step. This was especially significant for the smaller forces (0 – 2 N), where the change in frequency was particularly drastic and easily identifiable on the recorded frequency results. When forces larger than 10 N were applied, the changes were slower and less frequent. In other words, when applying 10 to 12 N, for example, there was no significant change in frequency. These gaps where no change of frequency was seen became larger as

more force was applied, to where no change in frequency was noticed with a 100 N force increase. When the force applied reached above about 120 N, the recorded frequencies no longer changed at all. Thus, at this stage of the testing, it appeared that the force sensor was more accurate with small forces (0 – 10 N), and inaccurate for forces larger than 120 N.

Unlike the dips shown in Figure 39, it was also noted that, when large jumps in frequency occurred for larger forces, the recorded resonating frequency was not identifiable, due to the large and imprecise gaps. During such frequency readings, it was not uncommon for the dip in recorded frequency to be a straight line along 0.5 MHz, with no discernible lowest point. Initially, the force sensor's frequency, as well as the antenna, was tested using a standard network analyser. However, due to the size and cost of the equipment, and for safety reasons, the network analyser could not be moved to the MTS for testing. Therefore, a small portable network analyser was used instead, which could not automatically record values. It is not clear if the standard network analyser would be more accurate when measuring small changes in frequency, which may be considered in future research.

As previously stated, a belt was used to cover the force sensor and apply the force directly to the force sensor. As expected, the belt experienced stretching when large forces were applied to the test rig. This could also be a result of the holes punched into the belt to attach it onto the rig. During the experimental stage, where large forces were present (above 1200 N for the belt), the force did not remain constant. For example, when the MTS bottom fixture was moved downward to apply more force and stopped at 1200N, the force would lower to 1150 N within ten seconds, and continue to drop over time. This also occurred with the load cell underneath the force sensor. However, the frequency of the force sensor remained the same. As noted, the fact that all results were recorded manually could have resulted in inconsistent and inaccurate results, as not all the measurements were taken simultaneously. The belt losing tension did influence the results, and could be one of the reasons the experiments were inaccurate at larger forces.

The test rig could be improved by using a different method to attach the belt in future studies. Punching holes into the belt removes some material, which weakens the belt. Alternative methods to punching holes into the belt to fit the bolts through to attach the belt could also be investigated. The experiment set-up can also be improved by automating the process. The readings were taken manually, and the results may have been affected by human error. This could be avoided if a different network analyser were used, or if program is written to work with the network analyser and record the lowest frequency in the range at determined intervals. As both the load cells can record force readings along with time, it will make the readings easier and more accurate if the data sets were to be combined. However, the force sensor design is still considered a successful attempt, and thus a contribution made by the present study, and, with some improvements and further testing, could possibly be used for *in vivo* testing in future research.

This study focused on the method of directly measuring patellofemoral contact force. Therefore, it was decided to do testing on a mechanical rig, to ensure all the components including the force sensor and different patellar buttons were suitable for future *in vitro* testing. The test rig cannot simulate exact knee movement; therefore, the results obtained for the effect of patellar buttons of different thicknesses cannot be expected to be the same as in cadaver studies. No similar studies testing the effect of different patellar button thickness on test rigs could be found.

In achieving Research Objective 4, the present study found that the thickness of the patellar button has a statistically significant effect on the measured contact force of the patellar button. Very few studies were found that directly addressed the effect of patellar button thickness on the contact force experienced. No recent studies were found that directly investigated this topic.

The findings of the present study are aligned with those of Hsu *et al*. (1996), that the patellofemoral contact force increases as the knee flexion angle is increased, and that a larger contact force is present with a thicker patellar button. The results also indicated that a larger change in force can be seen at larger knee flexion angles.

The present study's findings differ from those of the study by Oishi *et al.* (1996), which indicated no significant difference between the different compressive forces during the use of patellar buttons of different thicknesses.

Future studies should include refining of the force sensor used, as well as the smaller force sensors that were designed during this project. This could aid in measuring the distribution of the contact force, which could be useful in the native knee, as forces are expected to shift laterally during knee flexion, as well as from distal to proximal. Future work should also include cadaver testing, as well as testing on an Oxford knee rig similar to the one demonstrated in Figure 9.

7 Conclusion

The aim of the present study was to directly measure patellofemoral contact force as experienced by the patellar button, and a force sensor able to do so was designed. However, the design of the force sensor used in this project was found to be inaccurate. The force sensor was small enough to snugly fit in the patellar button, and was also measured wirelessly from distances up to 40 mm. However, the further aim of the study, that the force sensor would measure up to 1 kN, was not achieved, as the force sensor was only able to measure up to 120 N.

A test rig was successfully designed to both calibrate and characterise the force sensor, as well as measure the patellofemoral contact force experienced by patellar buttons of different thicknesses.

The difference in the thickness of the patellar buttons proved to have a significant effect on the simulated patellofemoral contact force. This is evidence that overstuffing the patellofemoral joint may significantly increase the patellofemoral contact force, which could lead to further problems, specifically anterior knee pain.

8 References

Alcerro, J.C., Rossi, M.D. & Lavernia, C.J. 2017. Primary total knee arthroplasty: How does residual patellar thickness affect patient-oriented outcomes? *The Journal of Arthroplasty*. 32(12):3621–3625.

Arden, N. & Nevitt, M.C. 2006. Osteoarthritis: Epidemiology. *Best Practice & Research Clinical Rheumatology*. 20(1):3–25.

Becker, R., Bonnin, M. & Hofmann, S. 2011. The painful knee after total knee arthroplasty. *Knee surgery, sports traumatology, arthroscopy*. 19(9):1409–1410.

Brechter, J.H. & Powers, C.M. 2002. Patellofemoral joint stress during stair ascent and descent in persons with and without patellofemoral pain. *Gait & posture*. 16(2):115–123.

Browne, C., Hermida, J.C., Bergula, A., Colwell, C.W. & D'Lima, D.D. 2005. Patellofemoral forces after total knee arthroplasty: effect of extensor moment arm. *The Knee*. 12(2):81–88.

Carreiro, J.E. 2009. Chapter Six - Lower leg. In J.E.B.T.-P.M.M. Carreiro (ed.). Edinburgh: Churchill Livingstone. 273–327.

Digikalla.info. 2017. *Tendons in the knee*. [Online], Available: digikalla.info/tendons-in-the-knee/tendons-in-the-knee-knee-tendons-and-ligamnets-knee-anatomy-the-orthopedic-sports-download/.

Dion, M.K., Healey, C.P., Giddings, S.L., Drazan, J.F., Roberts, J., Cady, N. & Ledet, E.H. 2015. Force measurement across the patellofemoral joint using a smart patellar implant following a total knee arthroplasty. In *2015 41st Annual Northeast Biomedical Engineering Conference (NEBEC)*. 1–2.

Drazan, J.F., Abdoun, O.T., Wassick, M.T., Dahle, R., Beardslee, L., Marcus, G.A., Cady, N.C. & Ledet, E.H. 2018. Simple implantable wireless sensor platform to measure pressure and force. *Medical engineering & physics*. 59:81–87.

Fairview. n.d. *Knee Pain with Uncertain Cause*.

Glyn-Jones, S., Palmer, A.J.R., Agricola, R., Price, A.J., Vincent, T.L., Weinans, H. & Carr, A.J. 2015. Osteoarthritis. *The Lancet*. 3.

Hamilton, W.G., Ammeen, D.J., Parks, N.L., Goyal, N., Engh, G.A. & Engh, C.A. 2017. Patellar Cut and Composite Thickness: The Influence on Postoperative Motion and Complications in Total Knee Arthroplasty. *The Journal of Arthroplasty*. 32(6):1803–1807.

Heino Brechter, J. & Powers, C.M. 2002. Patellofemoral stress during walking in

persons with and without patellofemoral pain. *Medicine and science in sports and exercise*. 34(10):1582–1593.

Horng-Haung, H., Zong-Ping, L., James, R. & Kai-Nan, A. 1996. Influence of patellar thickness on patellar tracking and patellofemoral contact characteristics after total knee arthroplasty. *The Journal of Arthroplasty*. 11(1):69–80.

Hungerford, D.S. & Barry, M. (in press). Biomechanics of the patellofemoral joint. *Clinical Orthopaedics and Related Research*. (144):9—15. [Online], Available: http://europepmc.org/abstract/MED/535256.

Kaneko, T., Kono, N., Mochizuki, Y., Hada, M., Sunakawa, T., Ikegami, H. & Musha, Y. 2018. The influence of compressive forces across the patellofemoral joint on patient-reported outcome after bi-cruciate stabilized total knee arthroplasty. *The Bone & Joint Journal*. 100-B(12):1585–1591.

Konno, T., Onodera, T., Nishio, Y., Kasahara, Y., Iwasaki, N. & Majima, T. 2014. Correlation Between Knee Kinematics and Patellofemoral Contact Pressure in Total Knee Arthroplasty. *The Journal of Arthroplasty*. 29(12):2305–2308.

Kovacevic, N. & Kaufman, K. 1995. *Patent No. 5425775*. [Online], Available: http://www.freepatentsonline.com/5425775.html.

Loudon, J.K. 2016. Biomechanics and Pathomechanics of the Patellofemoral Joint. *International journal of sports physical therapy*. 11(6):820–830. [Online], Available: https://www.ncbi.nlm.nih.gov/pubmed/27904787.

Matz, J., Lanting, B.A. & Howard, J.L. 2019. Understanding the patellofemoral joint in total knee arthroplasty. *Canadian journal of surgery. Journal canadien de chirurgie*. 62(1):57–65.

Miller, R.K., Goodfellow, J.W., Murray, D.W. & O'Connor, J.J. 1998. In vitro measurement of patellofemoral force after three types of knee replacement. *The Journal of Bone and Joint Surgery. British volume*. 80-B(5):900–906.

Moses, K.P. 2013. *Atlas of Clinical Gross Anatomy*. 2nd Ed. ed. K.P. Moses & ClinicalKey (eds.). Philadelphia, PA: Elsevier/Saunders.

Navarro, M.S., Beltrani Filho, C.A., Akita Junior, J., Navarro, R.D. & Cohen, M. 2010. RelaÃ§Ã\poundso entre o ligamento patelofemoral lateral e a largura da faceta patelar lateral. *Acta OrtopÃ\copyrightdica Brasileira*. 18:19–22. [Online], Available: http://www.scielo.br/scielo.php?script=sci_arttext&pid=S1413-78522010000100003&nrm=iso.

Oishi, C.S., Kaufman, K.R., Irby, S.E. & Colwell, C.W. 1996. Effects of patellar

thickness on compression and shear forces in total knee arthroplasty. *Clinical Orthopaedics and Related Research*. 331:283–290.

Petersen, W., Rembitzki, I.V., Brüggemann, G.-P., Ellermann, A., Best, R., Koppenburg, A.G.- & Liebau, C. 2014. Anterior knee pain after total knee arthroplasty: a narrative review. *International Orthopaedics*. 38(2):319–328.

Pierce, T.P., Jauregui, J.J., Cherian, J.J., Elmallah, R.K., Harwin, S.F. & Mont, M.A. (in press). Is There an Ideal Patellar Thickness Following Total Knee Arthroplasty? *Orthopedics*. 39(1):187—92.

Powers, C.M., Chen, Y.-J., Farrokhi, S. & Lee, T.Q. 2006. Role of peripatellar retinaculum in transmission of forces within the extensor mechanism. *The Journal of bone and joint surgery. American volume*. 88(9):2042–2048.

Powers, C.M., Souza, R.B. & Fulkerson, J.P. 2016. Chapter 22 Patellofemoral Joint. In *Pathology and Intervention in Musculoskeletal Rehabilitation*. 798–835.

Putman, S., Boureau, F., Girard, J., Migaud, H. & Pasquier, G. 2019. Patellar complications after total knee arthroplasty. *Orthopaedics & Traumatology: Surgery & Research*. 105(1):S43–S51.

Reider, B., Marshall, J.L., Koslin, B., Ring, B. & Girgis, F.G. (in press). The anterior aspect of the knee joint. *The Journal of Bone and Joint Surgery. American volume*. 63(3):351—356. [Online], Available: http://europepmc.org/abstract/MED/7204430.

Reuben, J.D., McDonald, C.L., Woodard, P.L. & Hennington, L.J. 1991. Effect of patella thickness on patella strain following total knee arthroplasty. *Journal of Arthroplasty*.

Roussot, M.A. & Haddad, F.S. 2019. The evolution of patellofemoral prosthetic design in total knee arthroplasty: how far have we come? *EFORT Open Reviews*. 4(8):503–512.

Sawaguchi, N., Majima, T., Ishigaki, T., Mori, N., Terashima, T. & Minami, A. 2010. Mobile-Bearing Total Knee Arthroplasty Improves Patellar Tracking and Patellofemoral Contact Stress: In Vivo Measurements in the Same Patients. *The Journal of Arthroplasty*. 25(6):920–925.

Schindler, O.S. 2012. Basic kinematics and biomechanics of the patellofemoral joint part 2: the patella in total knee arthroplasty. *Acta orthopaedica Belgica*. 78(1):11–29.

Scott, W.N. & Insall, J.N. 2012. *Insall & Scott surgery of the knee*. 5th Ed. ed. W.N. Scott, J.N. Insall, & ClinicalKey (eds.). Philadelphia, PA: Elsevier/Churchill Livingstone.

Tanikawa, H., Tada, M., Harato, K., Okuma, K. & Nagura, T. 2017. Influence of Total Knee Arthroplasty on Patellar Kinematics and Patellofemoral Pressure.

The Journal of Arthroplasty. 32(1):280–285.

Terashima, T., Onodera, T., Sawaguchi, N., Kasahara, Y. & Majima, T. 2015. External rotation of the femoral component decreases patellofemoral contact stress in total knee arthroplasty. *Knee Surgery, Sports Traumatology, Arthroscopy*. 23(11):3266–3272.

"Total knee arthroplasty". 2016. *AORN Journal*. 104(5):10–12.

Vos, T., Flaxman, A.D., Naghavi, M., Lozano, R., Michaud, C., Ezzati, M., Shibuya, K., Salomon, J.A., et al. 2012a. Years lived with disability (YLDs) for 1160 sequelae of 289 diseases and injuries 1990–2010: a systematic analysis for the Global Burden of Disease Study 2010. *The Lancet*. 380(9859):2163–2196.

Xu, C., Chu, X. & Wu, H. 2007. Effects of patellar resurfacing on contact area and contact stress in total knee arthroplasty. *The Knee*. 14(3):183–187.

Appendix A: Test rig components

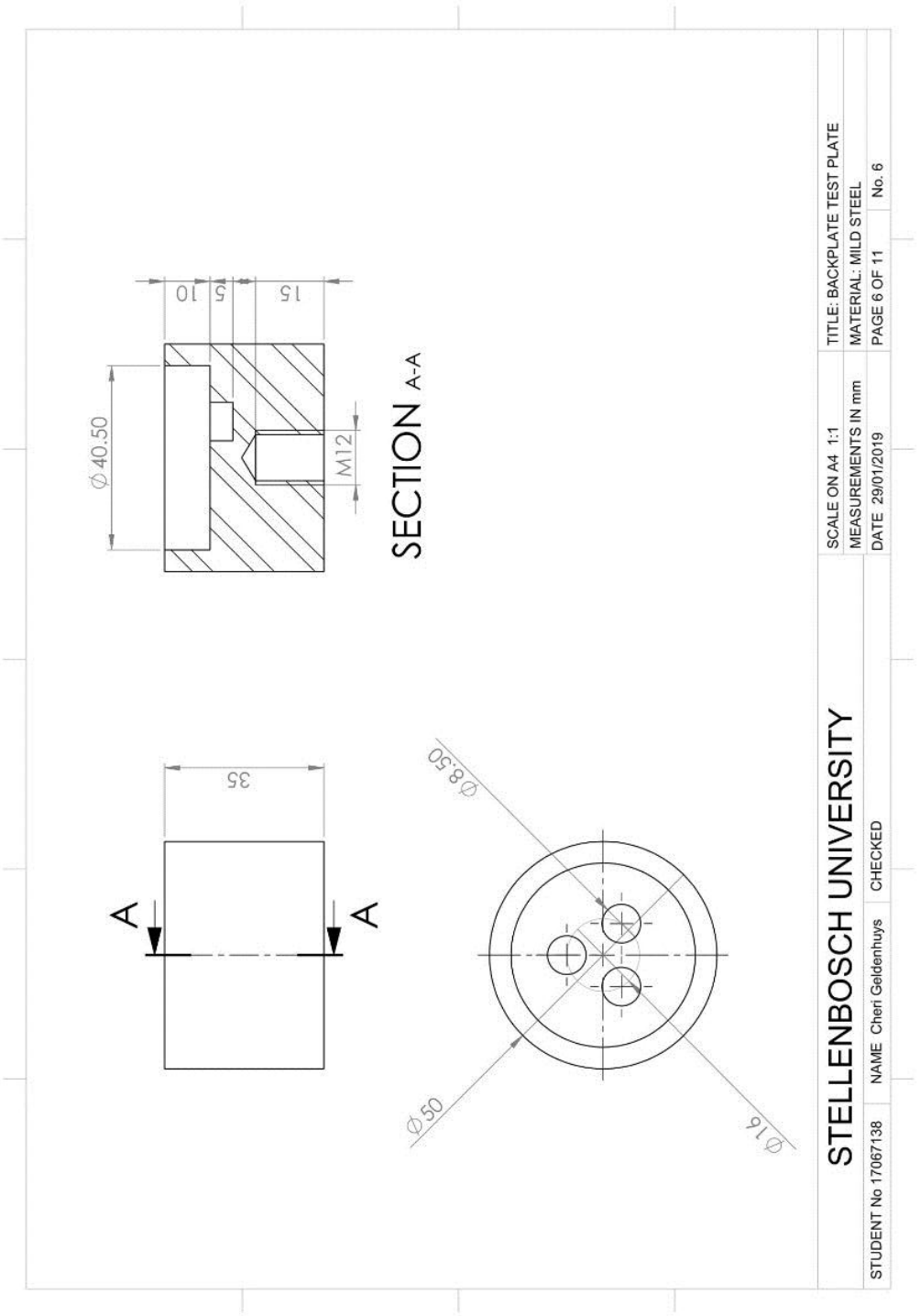

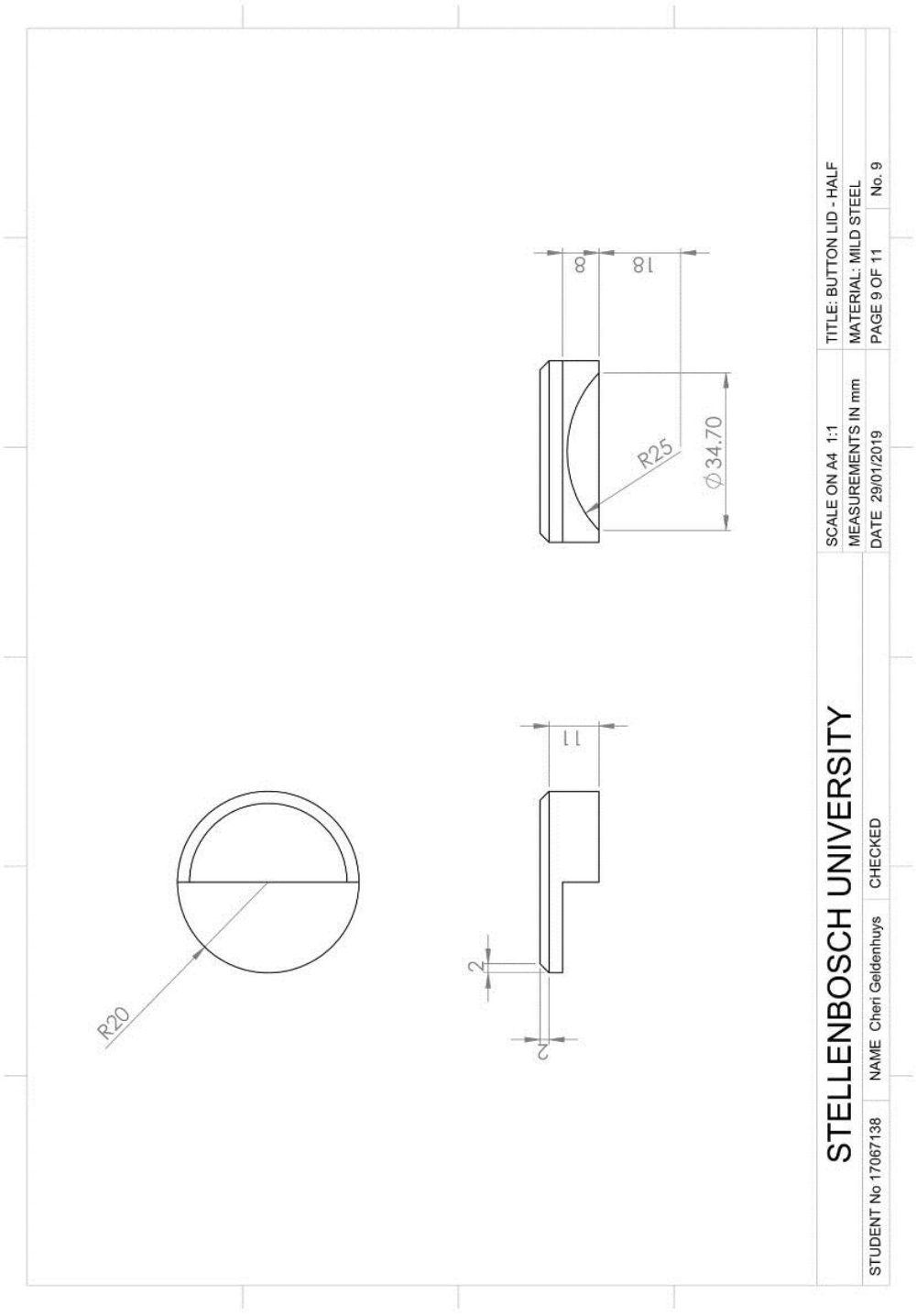

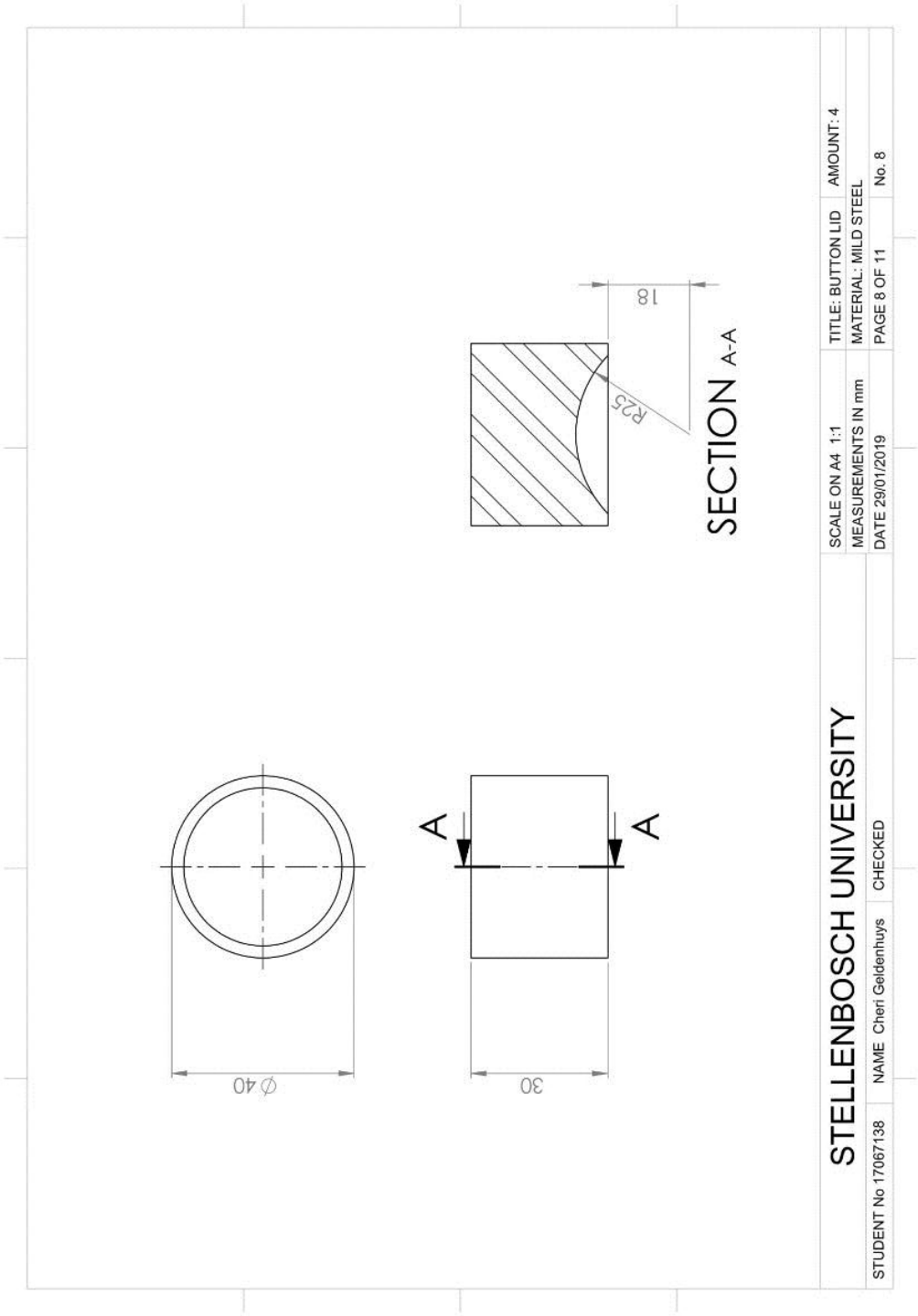

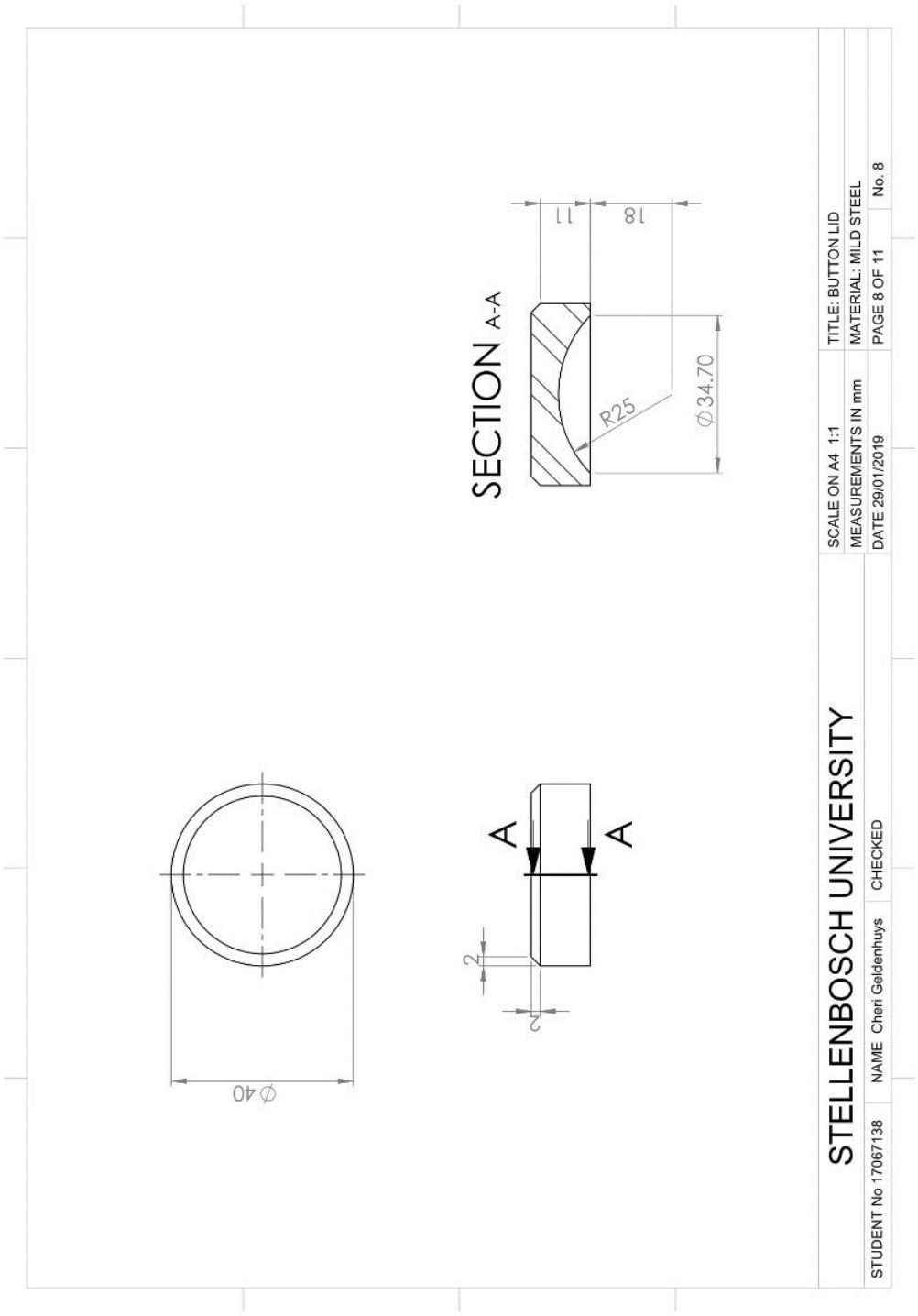

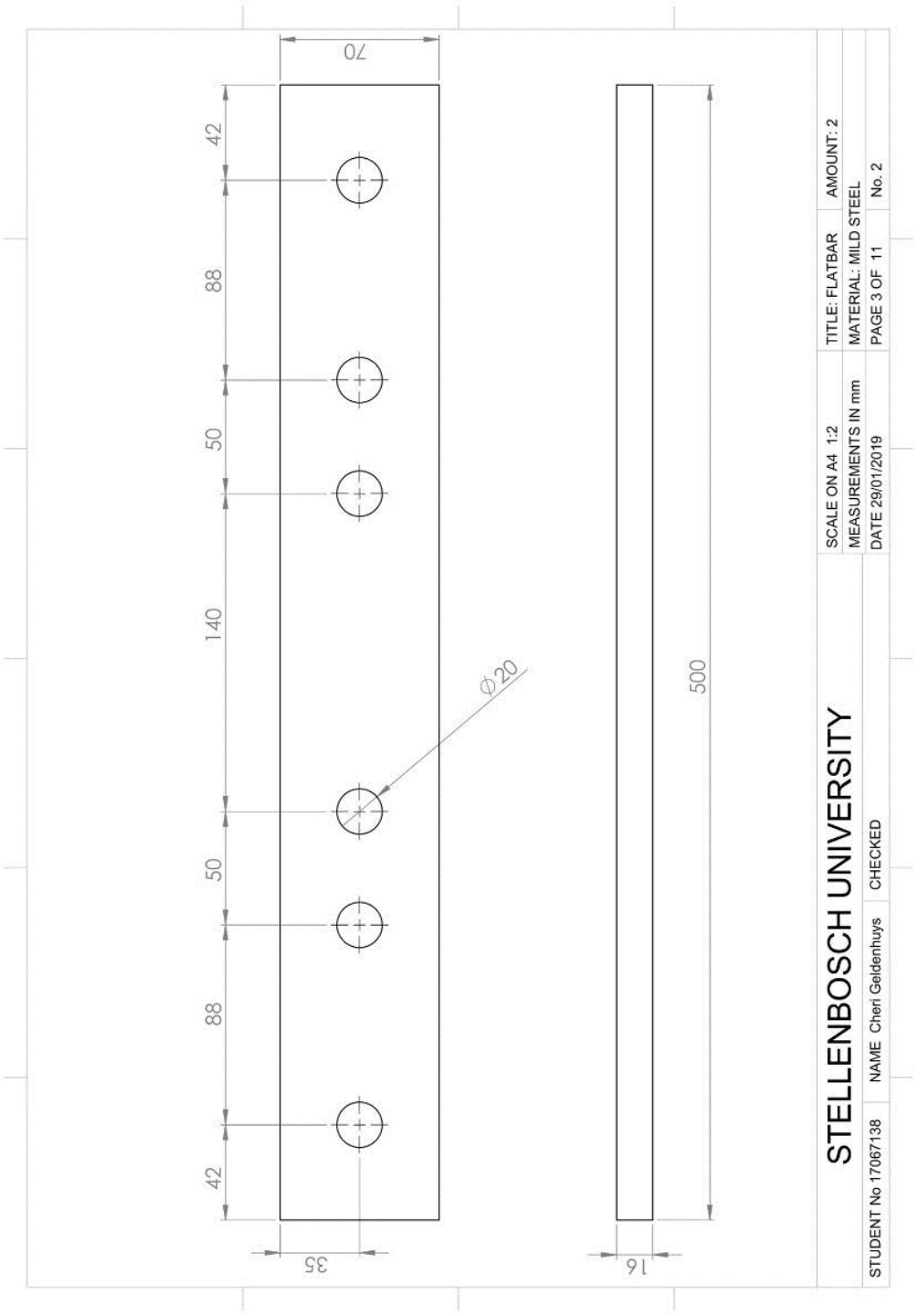

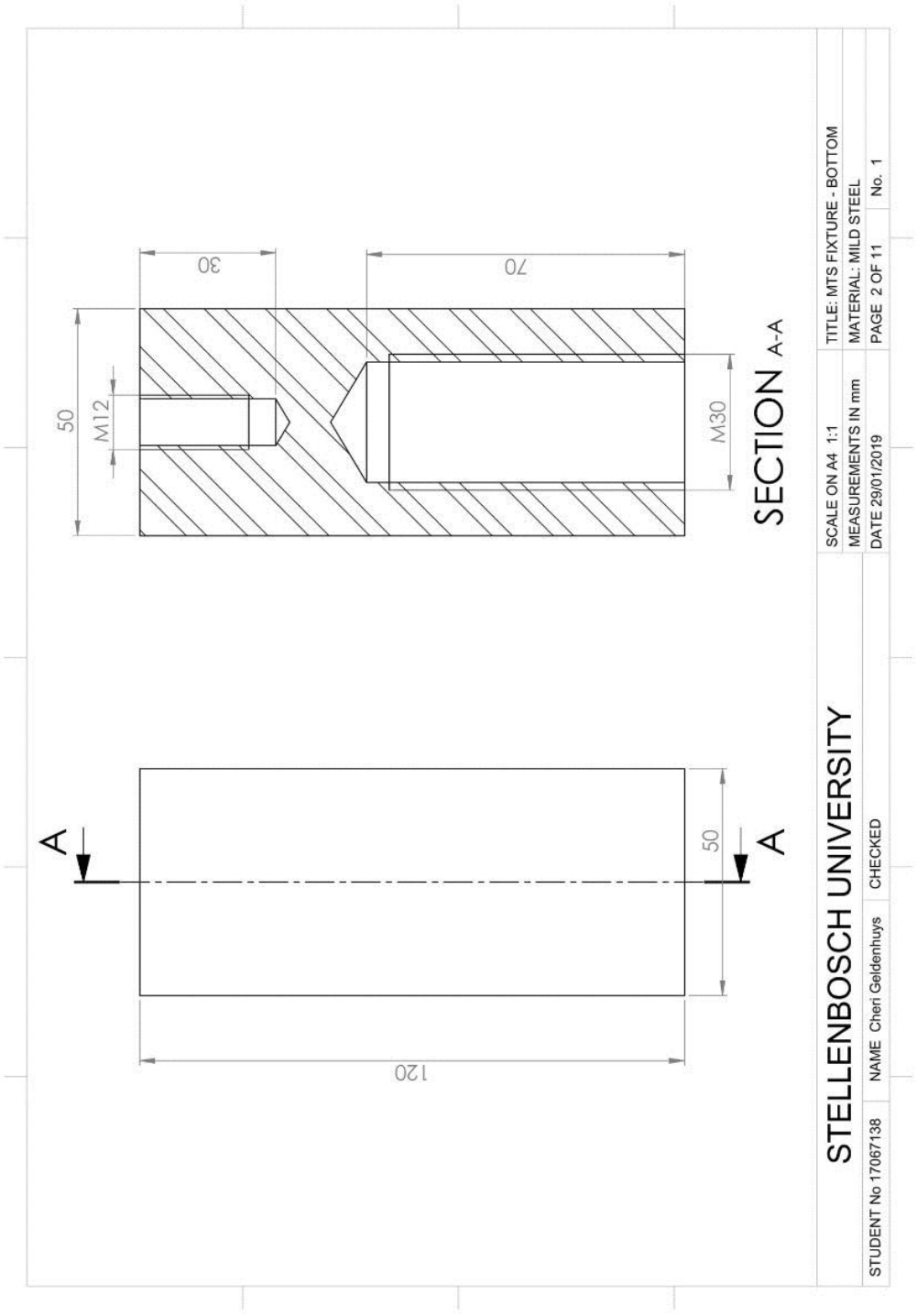

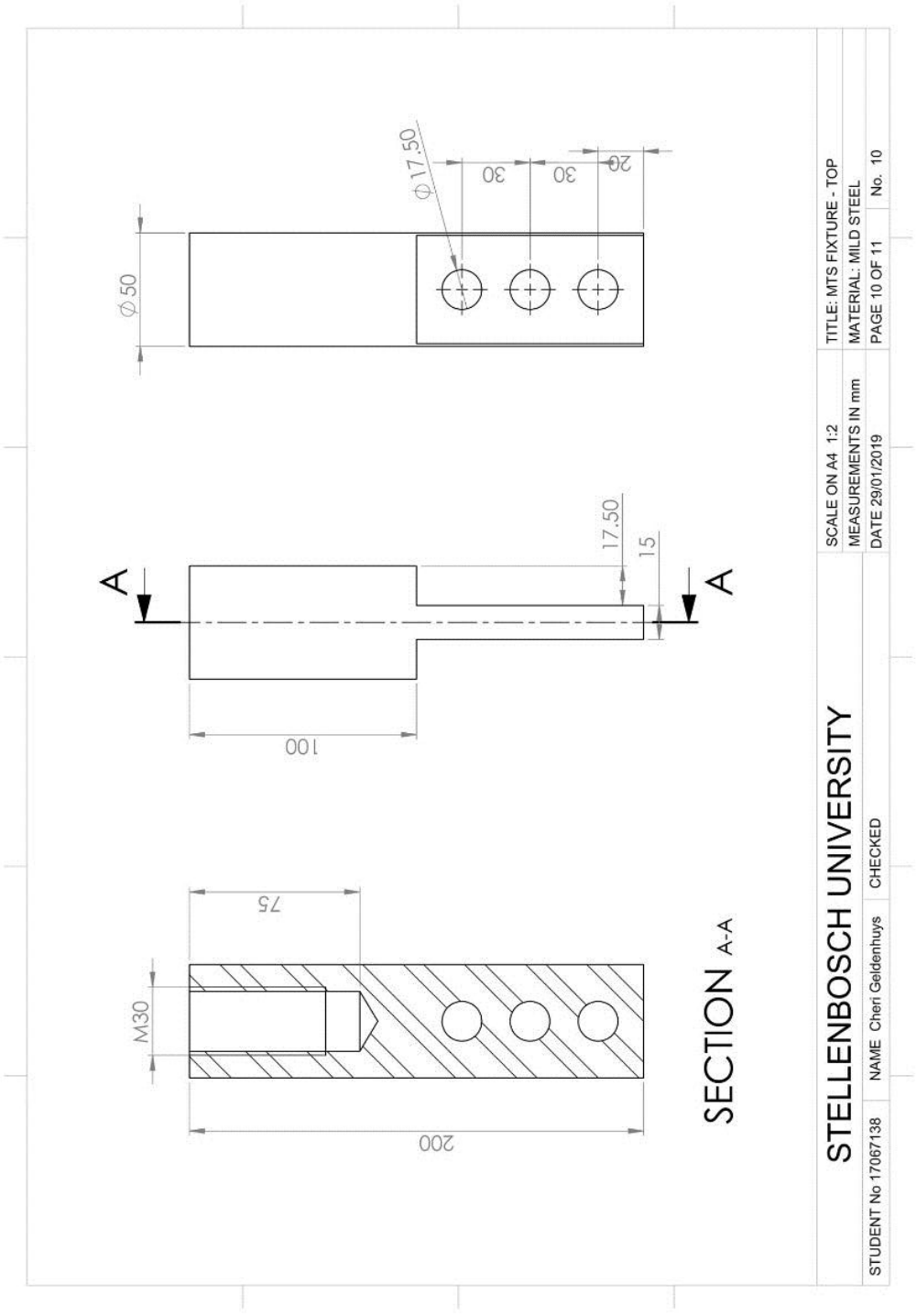

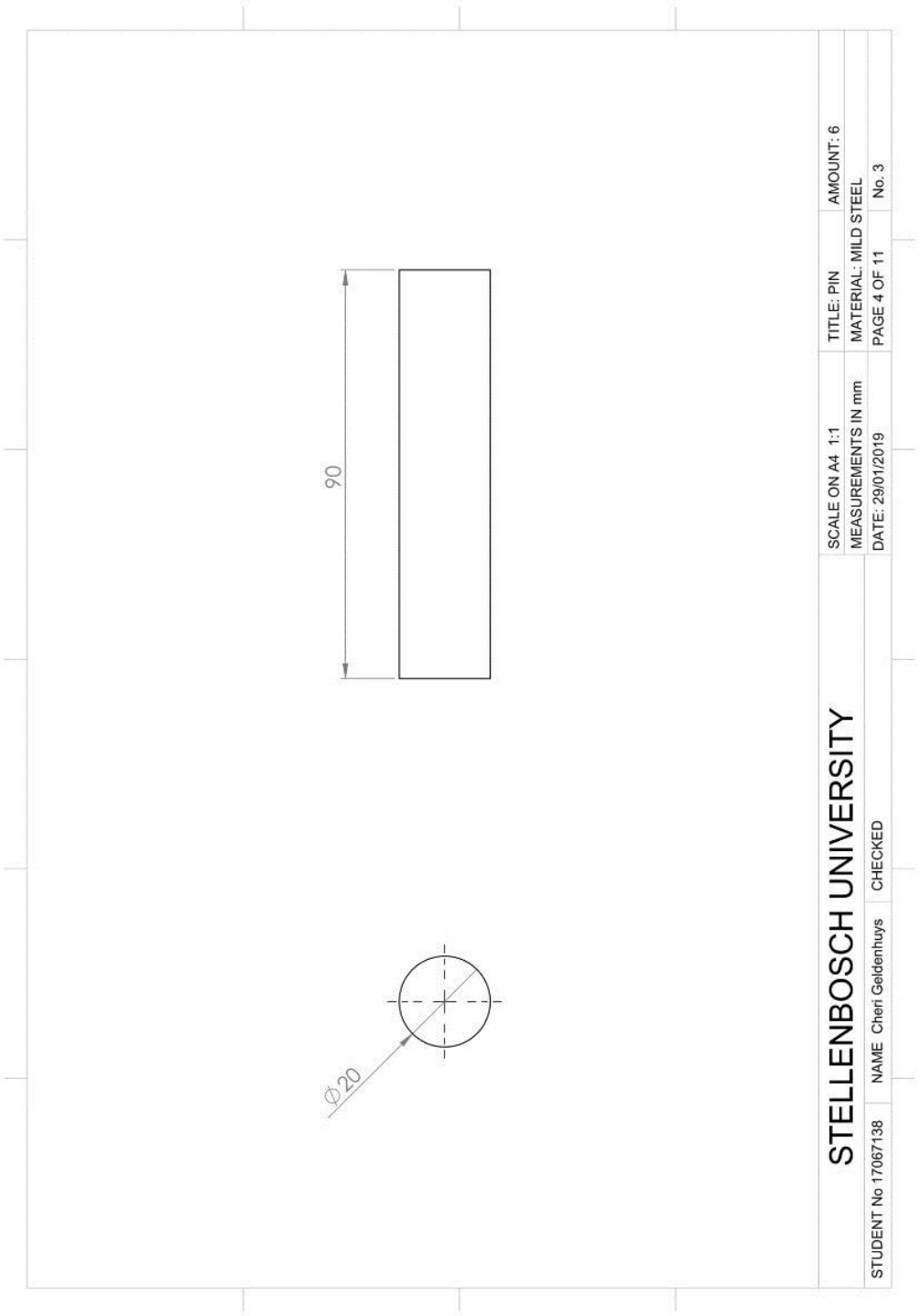

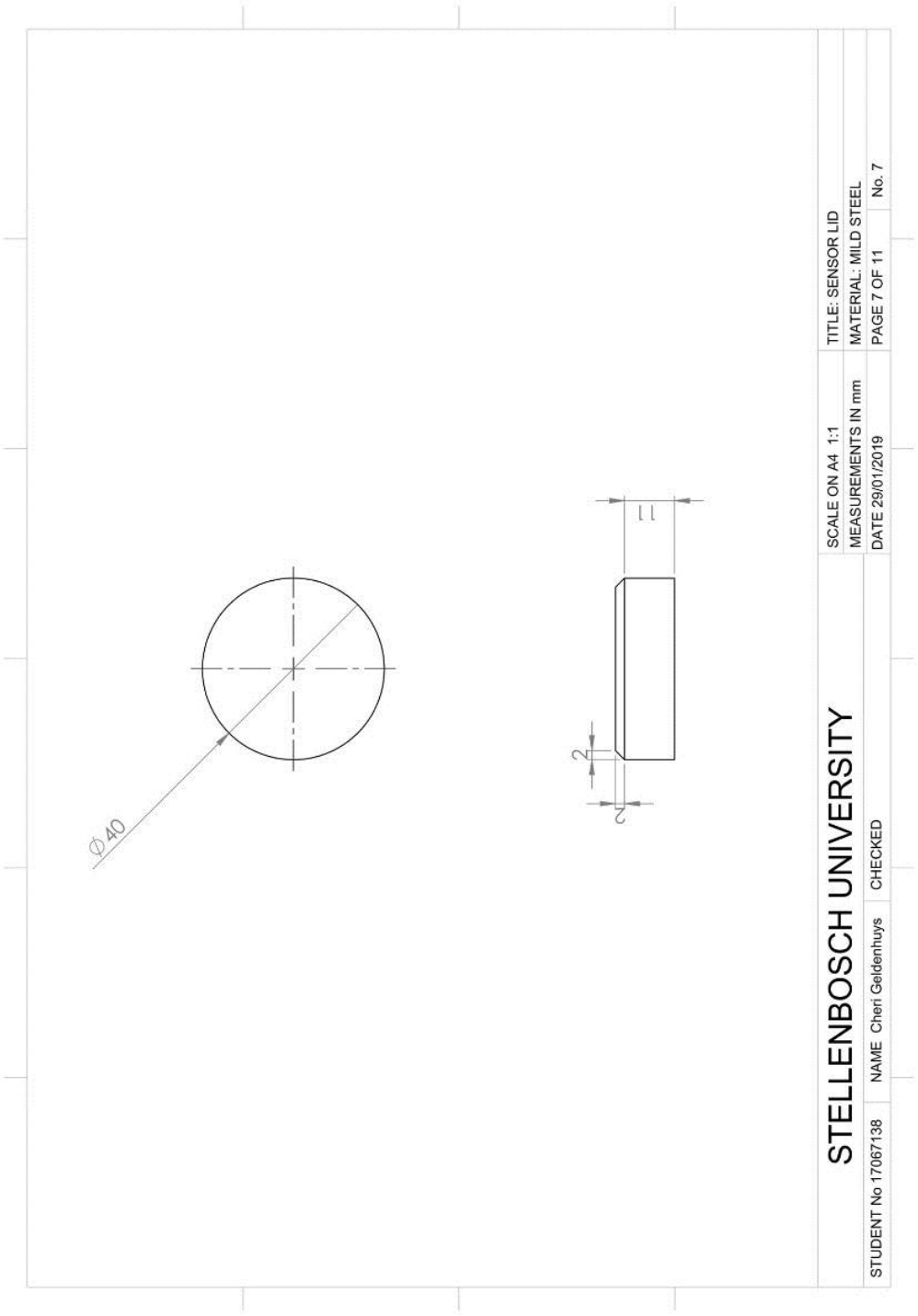

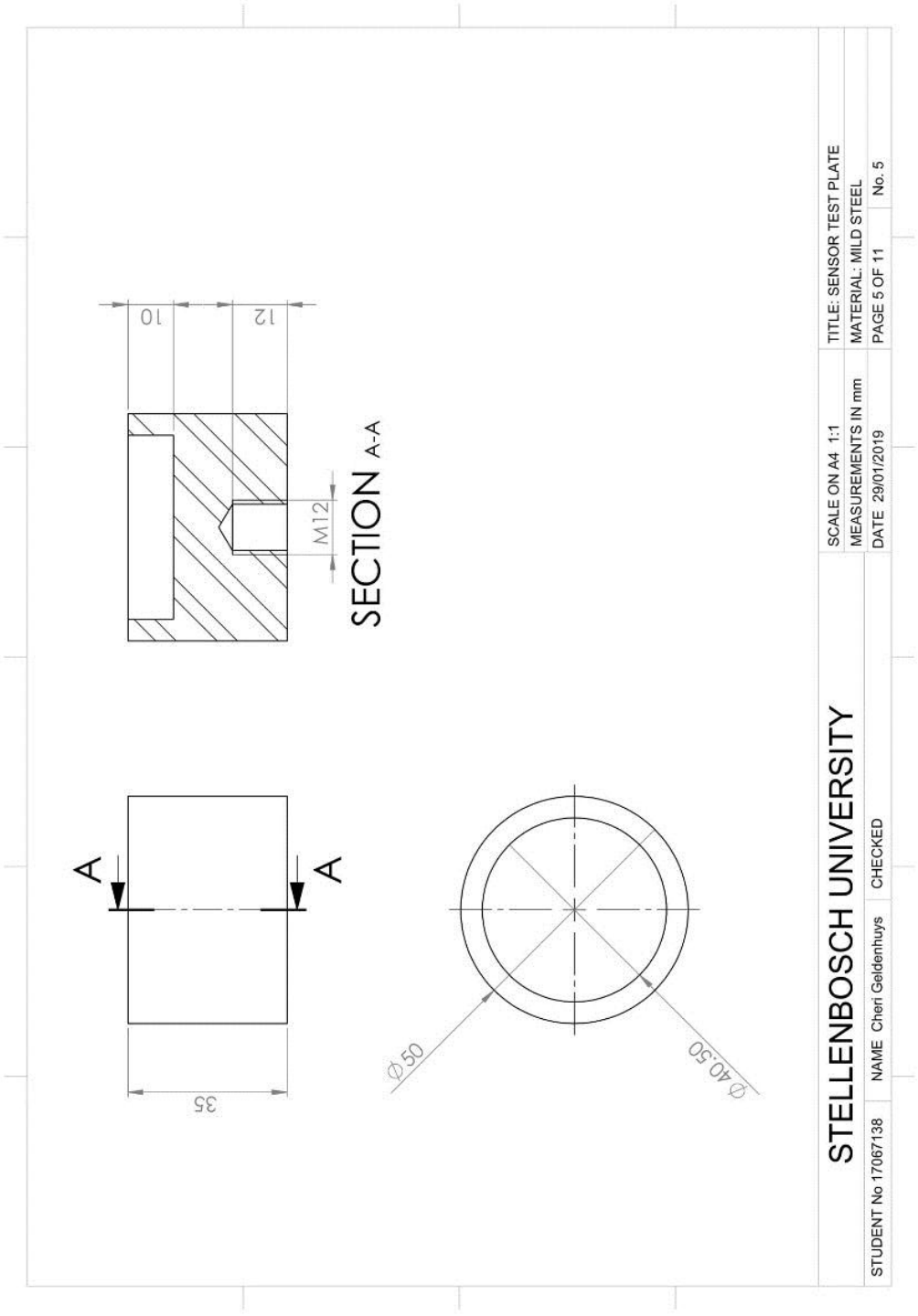

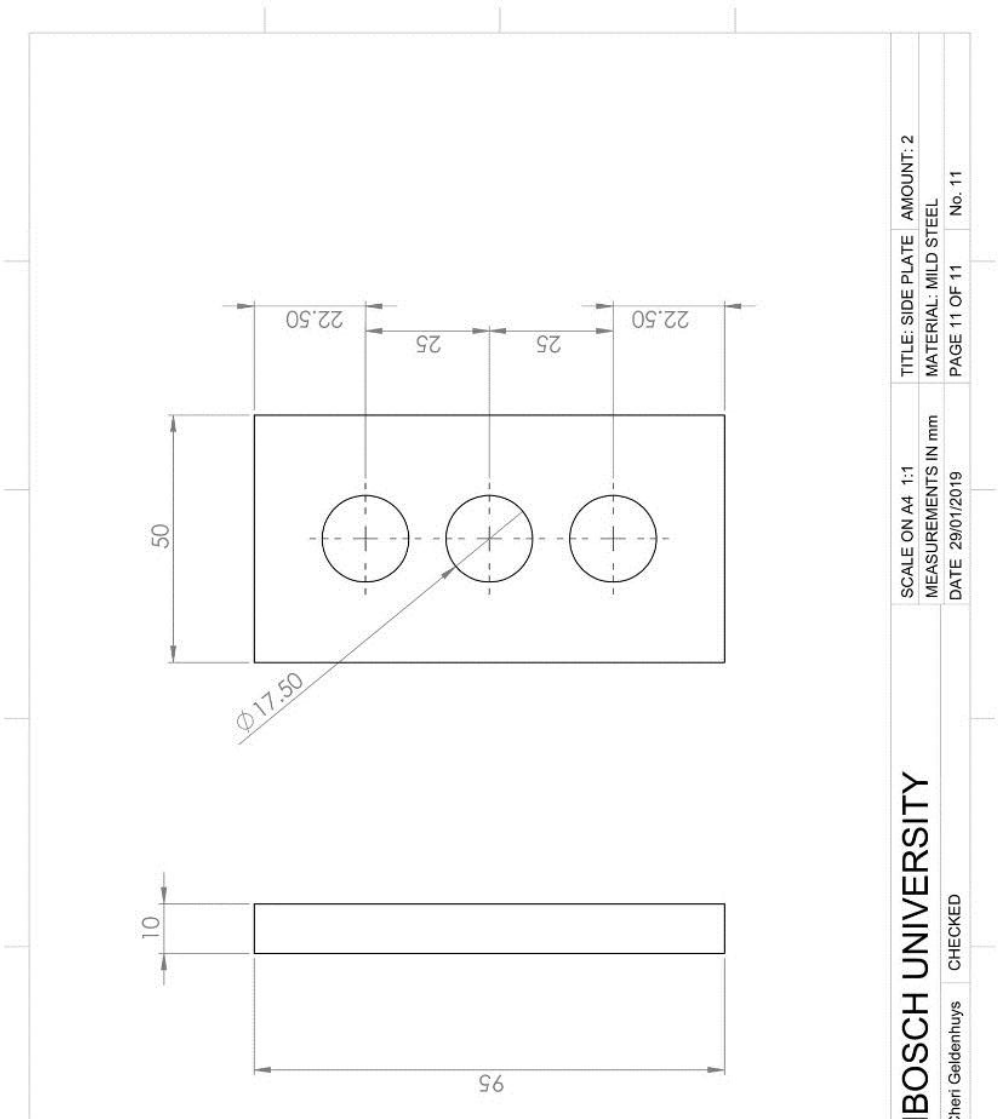

Appendix B: Patellar button and back plate design

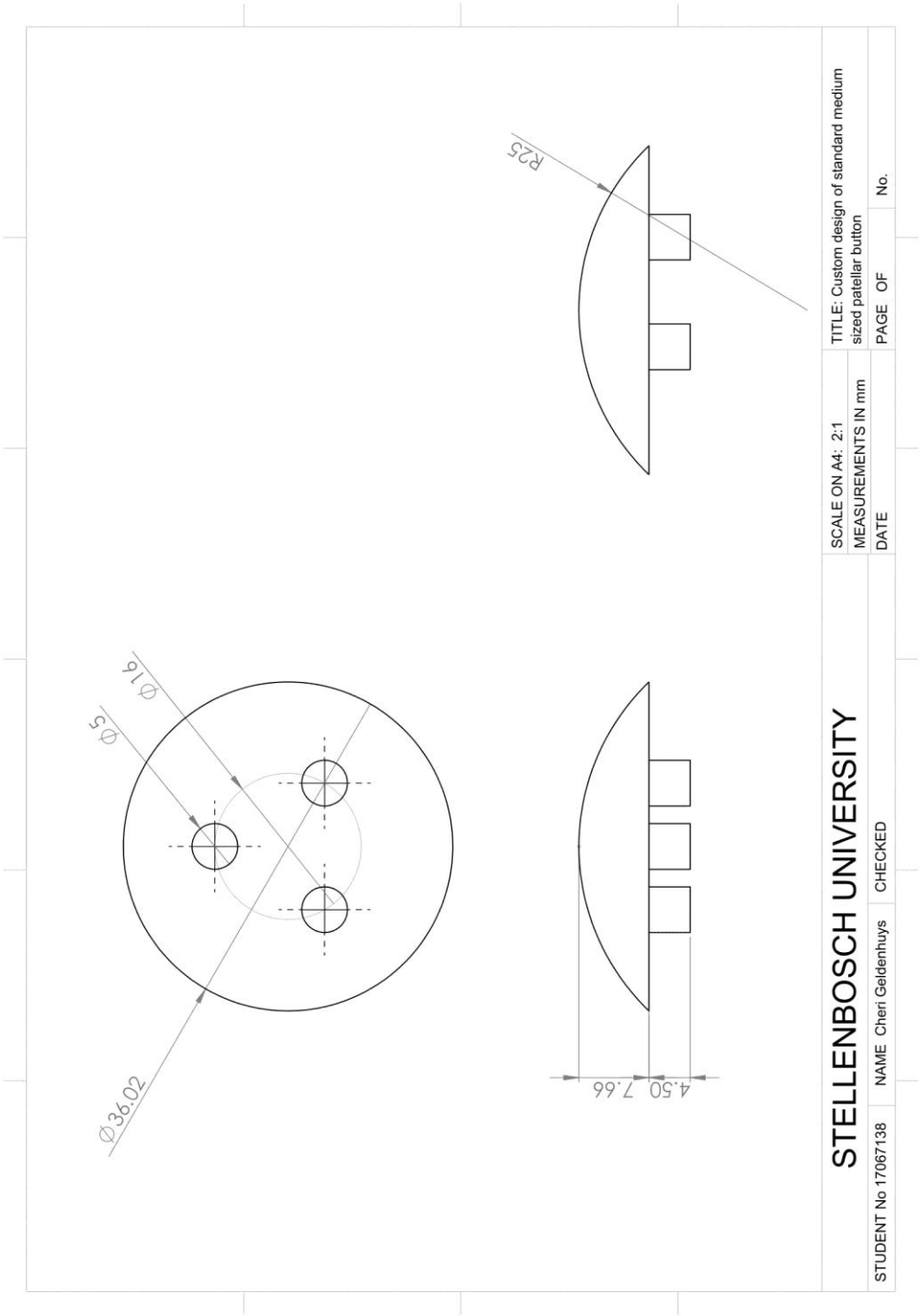

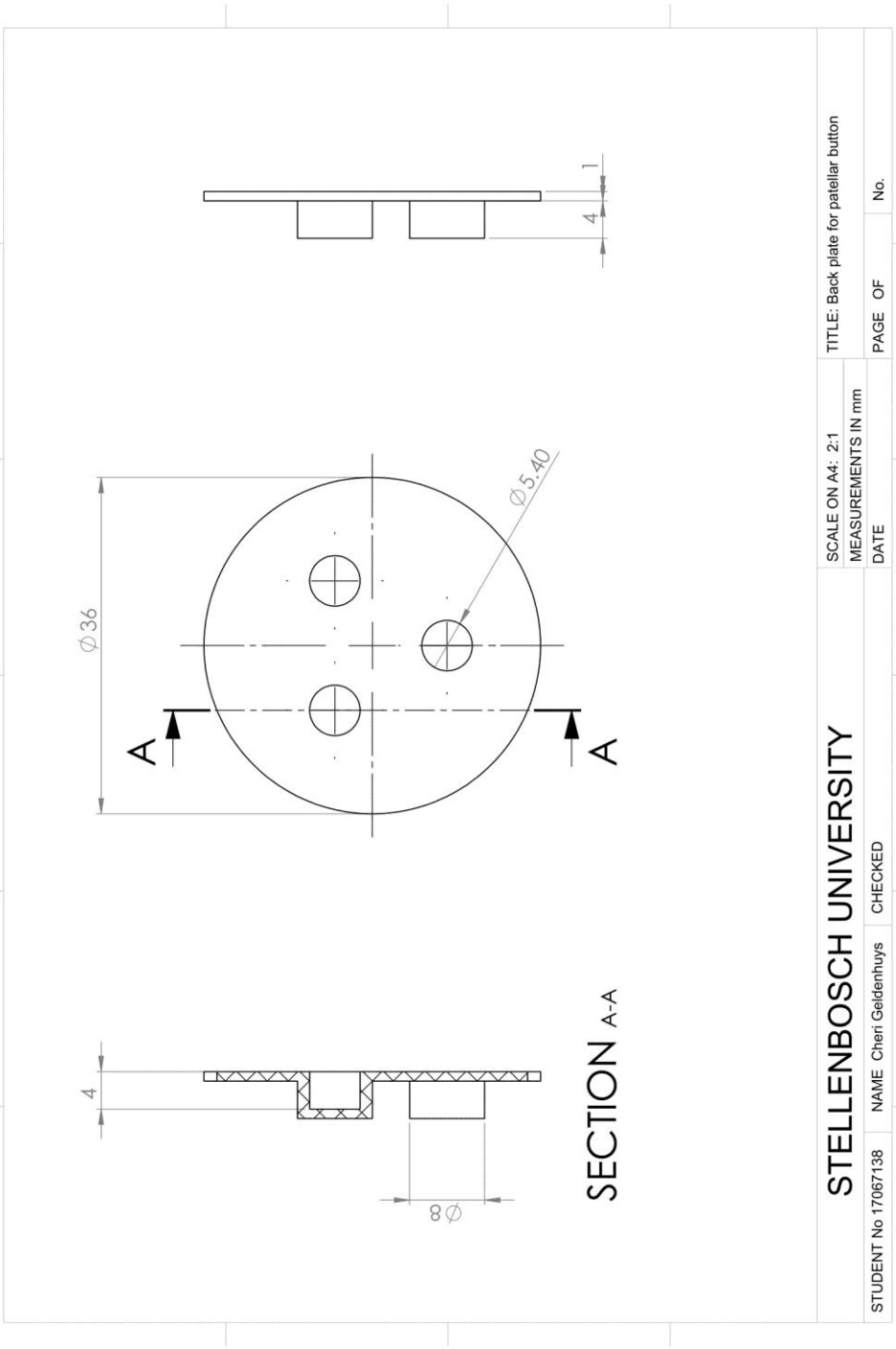

Appendix C: Load cell fact sheet

HBM

U2A_1T

Load cell

2D Derivation

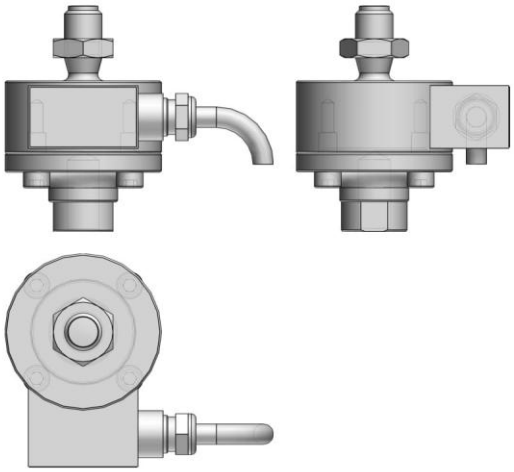

ISO View

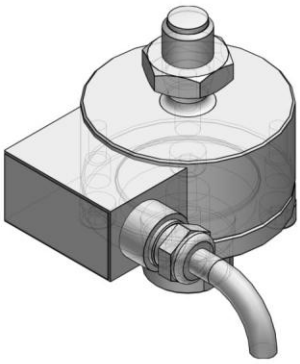

HBM

U2A_1T

Load cell

Technical Drawings

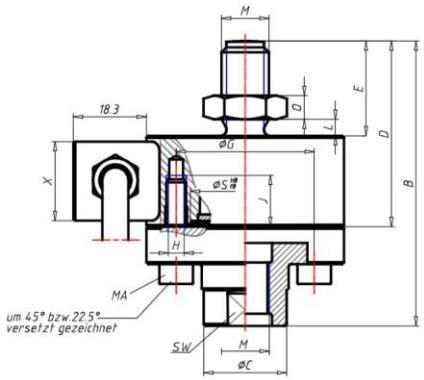

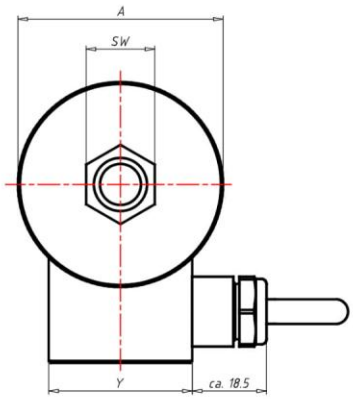

HBM

U2A_1T

Load cell

Technical Data

ORDERNO (Order No.)	1-U2AD1/1T
DRAWNO (Drawing No.)	B 1001-4.2
TYP (Type)	U2A
CAPACITY (Maximum capacity in t)	1t
A (ØA -0.2 / mm)	50
B (/ mm)	72
C (ØC / mm)	21
D (/ mm)	47
E (/ mm)	24
G (ØG / mm)	42
H (Thread)	4xM5
J (/ mm)	13
L (min / mm)	7.4
M (Thread)	M12
O (/ mm)	6
S (ØS H8 f8 / mm)	34
SW (/ mm)	19
X (/ mm)	20
Y (/ mm)	35
MA (/ N-m)	5

Appendix D: MATLAB code

```
%Creating a calibration curve for the force sensor
clear
clc
%Import 6 sets of calibration test data
%consisting of load cell [N] and force sensor data [MHz]
data1 = xlsread('Calibration.xlsx',1);
data2 = xlsread('Calibration.xlsx',2);
data3 = xlsread('Calibration.xlsx',3);
data4 = xlsread('Calibration.xlsx',4);
data5 = xlsread('Calibration.xlsx',5);
data6 = xlsread('Calibration.xlsx',6);
%create one matrix with all six tests data
data = [data1; data2; data3; data4; data5; data6];
%sort the entire set of data from smallest to largest
data = sortrows(data);
%seperate the two columns
x1 = data1(:,1);
y1 = data1(:,2);
x2 = data2(:,1);
y2 = data2(:,2);
x3 = data3(:,1);
y3 = data3(:,2);
x4 = data4(:,1);
y4 = data4(:,2);
x5 = data5(:,1);
y5 = data5(:,2);
x6 = data6(:,1);
y6 = data6(:,2);
%create seperate matrix for load cell data and sensor data
x = data(:,1);
y = data(:,2);
%plot the six different calibration curves seperately
plot (y1,x1)
hold on
plot (y2,x2)
hold on
plot(y3,x3)
hold on
plot(y4,x4)
hold on
plot(y5,x5)
hold on
plot(y6,x6)
xlabel ('Sensor frequency [MHz]')
ylabel ('Load cell force [N]')
title ('Characterisation curves')
```

```
hold off
%calculate correlation coefficient
r = corrcoef(data)
%create a function to best fit the data points
f = fit(y,x,'exp2');
%plot the data points together with the best fit curve
plot(f,y,x)
xlabel ('Sensor frequency [MHz]')
ylabel ('Load cell force [N]')
title ('Calibration curve')
hold off
%use the calibration curve function to calculate the force
experienced
%by the force sensor by entering the frequency of the force sensor
%and calculating the force experienced
z1 = f(y1);
z2 = f(y2);
z3 = f(y3);
z4 = f(y4);
z5 = f(y5);
z6 = f(y6);
```